Turbulence Measurements and Noise Generation

in a Transonic Cryogenic Wind Tunnel

by

Dwaine O. Griffith, II

Thesis submitted to the Faculty of the

Virginia Polytechnic Institute and State University

in partial fulfillment of the requirements for the degree of

Master of Science

in

Mechanical Engineering

APPROVED:

Dr. W. F. Ng, Chairman

Dr. J. Moore

Dr. C. L. Dancey

April 1989

Blacksburg, Virginia

Turbulence Measurements and Noise Generation

in a Transonic Cryogenic Wind Tunnel

by

Dwaine O. Griffith, II

Dr. W. F. Ng, Chairman

Mechanical Engineering

(ABSTRACT)

A high-frequency combination probe was used to measure dynamic flow quality in the test section of the NASA Langley 0.3-m Transonic Cryogenic Tunnel. The probe measures fluctuating stagnation (total) temperature and pressure, static pressure, and flow angles in two orthogonal planes. Simultaneous unsteady temperature and pressure measurements were also made in the settling chamber of the tunnel. The data show that the stagnation temperature fluctuations remain constant, and the stagnation pressure fluctuations increase by a factor of two, as the flow accelerates from the settling chamber to the test section. In the test section, the maximum rms value of the normalized fluctuating velocity is 0.7 percent. Correlation coefficients failed to show vorticity, entropy, or sound as the dominant mode of turbulence in the tunnel.

At certain tunnel operating conditions, periodic disturbances are seen in the data taken in the test section. A possible cause for the disturbances is found to be acoustic coupling of the test section and plenum chamber via the perforated side walls in the tunnel. The experimental data agree well with the acoustic coupling theory.

Acknowledgements

I would like to express my sincere respect and appreciation for my major professor, Dr. Wing-fai Ng. His extensive knowledge and management abilities proved invaluable in my research. He also performed the experiment on which this thesis is based.

Thanks are also extended to and helped Dr. Ng perform the experiment at NASA Langley, and helped reduce the data. knowledge of the computer system at Virginia Tech also helped to expedite my research.

The times that I have had with my many friends here in Blacksburg will never be forgotten. Their camaraderie and encouragement made life fun.

Finally, and most importantly, I would like to thank my family and my fiancee, . Their constant support, concern, and patience made it all worthwhile.

Table of Contents

List of Illustrations

List of Tables

Nomenclature

M	Mach number
P_T	total (stagnation) pressure
$P_{1,2,3,4}$	pressure as measured from transducer number 1, 2, 3 or 4
P	static pressure
$R_{u\rho}$	velocity and density correlation coefficient
R_{uT_T}	velocity and total temperature correlation coefficient
$R_{\rho T_T}$	density and total temperature correlation coefficient
T_T	total (stagnation) temperature
T	static temperature
u	freestream velocity
ρ	density
ρu	mass flux
α	angle of attack
β	angle of yaw
γ	ratio of specific heats

1.0 Introduction

The requirements to simulate full-scale flight Reynolds numbers in wind tunnels have prompted an effort to develop transonic tunnels with very high unit Reynolds numbers. The recent development and application of cryogenic wind tunnels, such as the U.S. National Transonic Facility (NTF) and the 0.3-m Transonic Cryogenic Tunnel (0.3-m TCT), represent a major advance in aerodynamic testing technology. Cryogenic tunnels, because of their extremely low temperatures, are able to develop very high unit Reynolds numbers. It was pointed out that the NTF should be used to establish the limit of the simulation capabilities of existing conventional ambient temperature (near atmospheric) wind tunnels [1]. This could be done by conducting pure Reynolds number studies ranging from the Reynolds numbers of the conventional wind tunnels up to the full-scale Reynolds numbers. In addition, due to the expense of cryogenic tunnels, experimentation in the future will continue to be done in existing ambient temperature tunnels [2]. It will therefore be important to correlate results obtained in the NTF with results obtained in conventional tunnels [2]. To this end the detailed documentation of dynamic flow quality in a transonic cryogenic wind tunnel becomes a prime research requirement for the cryogenic facilities.

Transonic cryogenic wind tunnels are by their very nature complex and sophisticated experimental tools. An assumption basic to wind tunnel testing is that a moving medium approaching a stationary aircraft (the wind tunnel case) is equivalent to the aircraft traveling through the stationary medium (the free-flight case). Thus the accuracy of the free-flight simulation depends on the quality of the flow in the test section. High levels of disturbances in the test section of wind tunnels can adversely affect aerodynamic data, making the data on models difficult to interpret. Experiments have shown that transonic wind tunnel disturbances may significantly influence boundary-layer transition and the character of buffet onset [3]. Thus, it is necessary to be able to measure the conditions in a given test section to ensure that consistent, smooth, uniform flow can be achieved. Of particular interest are the detailed time-resolved measurements of the turbulence intensities for velocity, temperature, and pressure fluctuations. For a number of years there has been a concerted effort to quantify the disturbance levels in subsonic and transonic wind tunnels. Owen [4] summarizes the results of a portion of this effort and discusses factors which can improve the flow quality in transonic wind tunnels.

Dynamic flow quality measurements had been made in a transonic cryogenic wind tunnel. Stainback [5] and Johnson [6] used a three-wire hot-wire probe with each wire operating at a different overheat ratio to measure the velocity, density, and total temperature fluctuations in the test section of the 0.3-m TCT. Besides difficulty associated with lengthy calibration and possible wire breakage, the measured turbulence intensities from three-wire probes are usually much higher than measured intensities from other types of probes [6]. In addition, flow angularity cannot be measured using this method. Ng and Rosson [7] used an aspirating temperature and pressure probe to measure turbulence intensities in the settling chamber and test

section of the 0.3-m TCT. However only limited data were obtained and they do not cover the entire operating envelope of the tunnel.

Ng and Gundappa [8] then used a recently developed combination probe to measure fluctuating total temperature and pressure, static pressure, and flow angularity in the 0.3-m TCT. Turbulence intensities in the settling chamber and test section of the tunnel, in terms of normalized total temperature and pressure fluctuations, were documented for the entire operating envelope of the tunnel. Test section flow angularity and Mach number fluctuations were also presented. The data from the combination probe were not fully reduced, however. The scope of this thesis is to further the data reduction as well as to analyze the data to identify the origin of noise generation in the tunnel. An error analysis on all reported quantities is also done in this thesis. Ng and Gundappa noticed that at certain tunnel operating conditions, the disturbances in the tunnel were very periodic. Another objective of this thesis is to determine the origin of the periodic disturbances.

In an effort to determine noise origins in a wind tunnel, possible sources must be identified. Tunnel blockage and shock wave reflections are known sources of poor flow quality in transonic wind tunnels. As a solution to these problems, many transonic tunnels use porous walls to connect the test section with a plenum chamber. Plenum suction is used to decrease the boundary layer in the test section, and thus reduce blockage. The holes in the wall also allow many of the shocks to pass through to the plenum chamber rather than be reflected back into the test section. A disadvantage of the porous walls, however, is that they create additional noise in the test section. Most research (Ref. [3] and Refs. [9]-[13]) has found that porous walls are the dominant source of noise in the test sections of tunnels. Edge

tones, vortices shed by the leading edge of the holes, are thought to be the mechanism by which the noise is generated. Disturbances created by the edge tones are then radiated outward into the test section. The edge tone disturbances are periodic in nature. Thus, resonance frequencies are created in the wind tunnel by the addition of porous side walls.

Experiments have shown that measurements taken near the tunnel resonance frequency are in considerable error. Research was therefore conducted to predict tunnel resonance frequencies generated by the porous side walls in a test section. Mabey [13] was able to predict the natural frequencies for tunnels with slotted and perforated walls connecting the test section with the plenum chamber. His theory agrees well with experiments in rectangular tunnels. Lee [12] then developed a finite-element method which predicts resonance frequencies for arbitrarily shaped test sections and plenum chambers. For the 0.3-m TCT experiment reported in this thesis, perforated side walls were used in the test section of the tunnel. Therefore, in the present work, resonance frequencies generated by the porous walls are examined as a possible source for the periodic disturbances observed in the tunnel.

The purpose of this thesis is to present the results of the 0.3-m TCT experiment, and to develop an explanation for the periodic disturbances observed in the tunnel. Brief descriptions of the combination probe and experimental setup are presented first, followed by a discussion of the results. The turbulence intensities in the settling chamber and test section of the tunnel, in terms of normalized total temperature and pressure fluctuations, are documented for the entire operating envelope of the tunnel. Test section Mach number, flow angularity, velocity, static temperature, and mass flux fluctuations are then presented. Next, resonance frequencies generated by the

porous side walls in the tunnel are investigated as a possible cause of the periodic disturbances. Whenever possible, data are compared with previous measurements in the tunnel for consistency. Finally, conclusions and recommendations are made.

2.0 Instrumentation

2.1 Aspirating Temperature and Pressure Probe

The combination probe used by Ng and Gundappa [8] in the 0.3-m TCT experiment consists essentially of two probes, a high-frequency aspirating probe, and a high frequency angle probe. The aspirating probe is piggyback-mounted on the angle probe as shown in Fig. 1. The aspirating probe consists of two coplanar constant temperature hot wires at different overheat ratios operated in a 1.5-mm (0.06-in.) diameter channel with a choked exit so that the flow past the wires is at a constant Mach number. Thus the mass flux by the wires is a function only of freestream total temperature and pressure and is not otherwise affected by changes in freestream velocity or density. The hot wires are operated in two separate constant temperature anemometer circuits. The governing equation for each hot wire can be put in the form (see Ref. [7])

$$V^2 = a\left[\frac{P_T}{\sqrt{T_T}}\right]^m (T_w - rT_T) \tag{2.1}$$

where P_T, and T_T are the total pressure and total temperature, respectively, V is the anemometer bridge voltage, T_w is the temperature of the hot wire, *r* is the ratio of static to total temperature, and *a* and *m* are empirically derived constants.

Calibration of the aspirating probe is done on-site by simultaneously recording the tunnel mean P_T and T_T, and the corresponding mean voltages from the hot wires at each tunnel condition. A functional relationship of the form of equation 2.1 can then be fitted to the calibration data, and the constants *a* and *m* determined for each wire. This represents the steady-state calibration of the aspirating probe.

After finding the calibration constants *a* and *m* for each wire, the correlation of equation 2.1 can be used to solve two equations for the two unknowns P_T and T_T . Time-resolved measurements can therefore be made. Further application and performance characteristics of the aspirating probe are given in Ref. [14].

2.2 *Angle Probe*

As shown in Fig. 1, the high-frequency aspirating probe is piggyback-mounted on a high-frequency angle probe. The angle probe is a four-sensor, 5.2-mm (0.2-in.) diameter pyramid type probe capable of simultaneously measuring the time-resolved stagnation and static pressures and two orthogonal flow angles (Fig. 1). The probe consists of surface-mounted silicon pressure sensors yielding a frequency response above 20 kHz.

The aerodynamic behavior of the angle probe with the piggyback aspirating probe was established by steady-state testing of a full-size model, with pressure taps at the

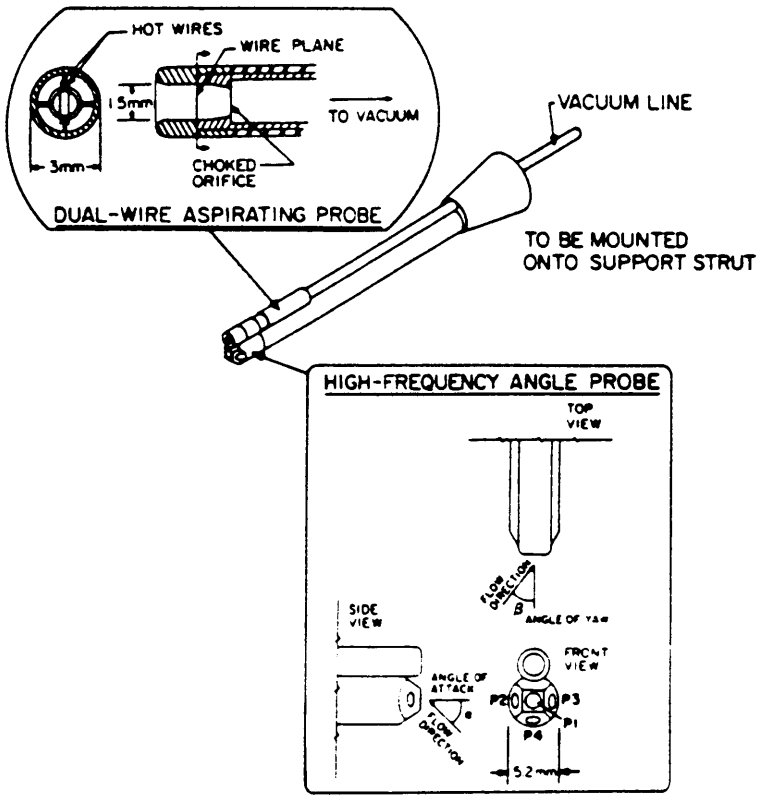

Figure 1. Combination Probe: Scale drawings of the combination probe including details of the aspirating probe (top) and the angle probe (bottom).

center of the flats representing the four diaphragms. A vacuum pump connected to the dummy aspirating probe showed that the effect of suction on calibration of the angle probe was negligible. The calibrations for the angle probe were carried out in an open jet of known conditions at Mach numbers 0.10, 0.24, 0.50, and 0.75. Calibration for angle of attack α (see Fig. 1) covered a range of ± 24 deg. Because of probe symmetry, the calibration for angle of yaw β covered only a range of 0 to $+24$ deg.

The measurements from the angle probe of the static and total pressures and the angles in two planes can be used to calculate the Mach number and its components in three directions. The Mach number can then be coupled with the total temperature from the aspirating probe to determine the static temperature. With these quantities known, the values of the velocity components, the density, and the mass flux can all be deduced. Further details of the combination probe's construction and calibration can be found in Ref. [15].

All semiconductor pressure transducers used in this experiment were calibrated for variations in both pressure and temperature. All data were digitized on-line at a rate of 100 kHz using a high speed A/D system. The data acquisition system was preceded by antialiasing 4-pole Bessel filters and amplifiers where appropriate. Further details on the data acquisition system can also be found in Ref. [15].

3.0 0.3-m TCT Experiment

3.1 Experimental Background

The 0.3-m Transonic Cryogenic Tunnel at NASA Langley Research Center is a fan-driven, closed-circuit wind tunnel using nitrogen as the working fluid (Fig. 2). The injection of liquid nitrogen into the tunnel circuit, just downstream of the test section, allows cryogenic total temperatures to be obtained. For steady operating conditions the heat of compression of the fan is removed by the injection of liquid nitrogen. Under equilibrium conditions the excess mass is removed from the circuit through an exhaust system located just upstream of the settling chamber. The test section is .33 m x .33 m (13 in. x 13 in.) with adaptive top and bottom walls for reducing blockage effects due to the presence of test models. In addition, the tunnel has perforated side walls for boundary layer removal. As mentioned previously, and described in more detail later, these perforated side walls could be the cause of the resonance which was observed during the experiment.

Measurements were taken at the following tunnel conditions, which represent the operating envelope of the tunnel:

$$0.30 < M < 0.85$$

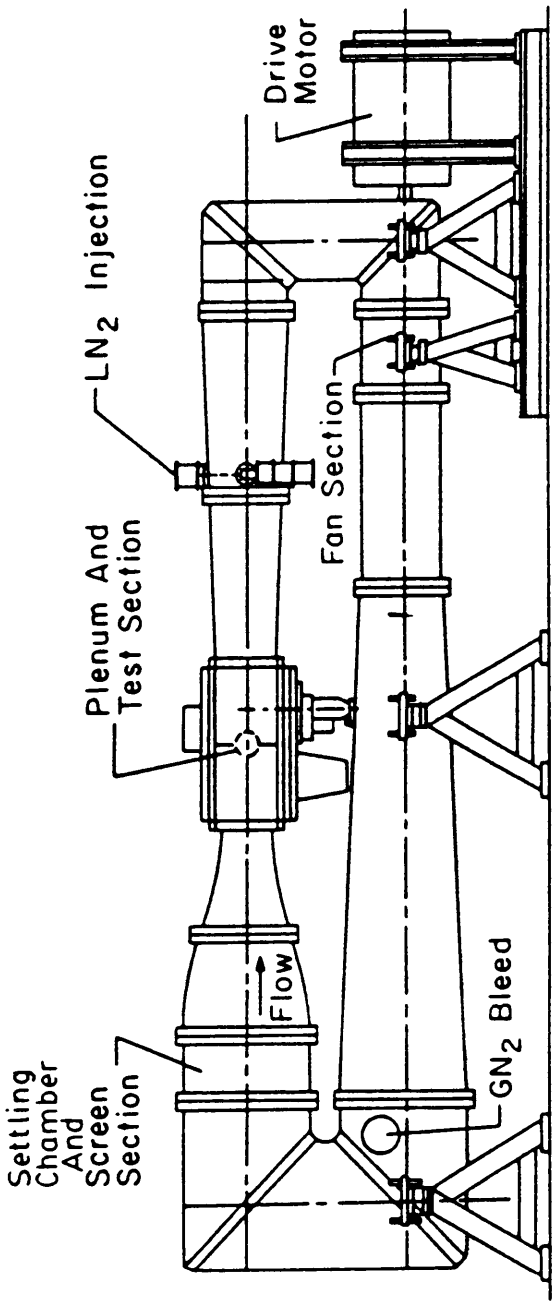

Figure 2. NASA Langley 0.3-m Transonic Cryogenic Tunnel

$$1.2 < P_T < 6 \text{ atm}$$

$$120\ (216) < T_T < 250\ \text{K}\ (450\ \text{R})$$

These conditions correspond to a Reynolds number range of

$$9.8 \times 10^6/\text{m}\ (3.0 \times 10^6/\text{ft}) \leq \text{Re/length} \leq 2.8 \times 10^8/\text{m}\ (85.0 \times 10^6/\text{ft})$$

The experiment began at the highest total temperature, 250 K (450 R), and a total pressure of 1.2 atm. Measurements were taken at various Mach numbers in the range given above. Without changing the total temperature, the total pressure was then increased to 2.0 atm, and the Mach number variation was repeated. This procedure was followed at total pressures of 3.0, 4.0, 5.0, and 6.0 atm. The total temperature was then lowered to 185 K (333 R) and 120 K (216 R), consecutively, and the above procedure was repeated at each temperature.

3.2 Probe Location

The combination probe was mounted in a rake in the freestream of the test section of the tunnel. The orientation of the probe was such that the angle of yaw (Fig. 1) corresponded to the angle measured in a plane parallel to the top and bottom walls of the tunnel. A high-frequency semiconductor pressure transducer was also mounted flush on the test section side wall to monitor the wall static pressure fluctuation.

A second aspirating temperature and pressure probe was mounted in the settling chamber of the tunnel. The probe was mounted downstream from the damping screens and was positioned in the freestream of the settling chamber. This provided

simultaneous turbulence measurements of total temperature and pressure in both the settling chamber and test section of the tunnel. Piggyback mounted with the aspirating probe in the settling chamber was a high-frequency impact probe, which consisted of a semiconductor pressure transducer mounted about one diameter away from the inlet of the impact probe. This provided an independent measurement of the fluctuating total pressure which could be used to check the measurements from the aspirating probe for consistency. Since the velocity in the settling chamber is very small, the measured fluctuating total pressure from the impact probe was almost the same as the fluctuating static pressure.

4.0 Experimental Results

As previously mentioned, periodic disturbances were observed at several tunnel operating conditions during the 0.3-m TCT experiment. The data with periodic disturbances are treated separately from the data with random turbulence, as they are different phenomena. The data exhibiting resonance are therefore not included in the rms summaries of the fluctuations which are presented in this chapter. Also, the turbulence data can be broken into two smaller groups. The first group consists of data from the individual probes comprising the combination probe: the aspirating probe, and the angle probe. The second group consists of data obtained by combining measurements from the two probes.

4.1 Turbulence Data

Typical raw data obtained from the angle probe are presented in Fig. 3, showing the four pressure measurements (P_1, P_2, P_3, P_4) from the transducers. The corresponding reduced data, in terms of static pressure, total pressure and two flow angles, are presented in Fig. 4. It can be seen that the peak-to-peak static and total pressure fluctuations are less than 1.4 kPa (0.2 psi) and the corresponding flow angle fluctuations in the yaw and pitch directions are less than one degree.

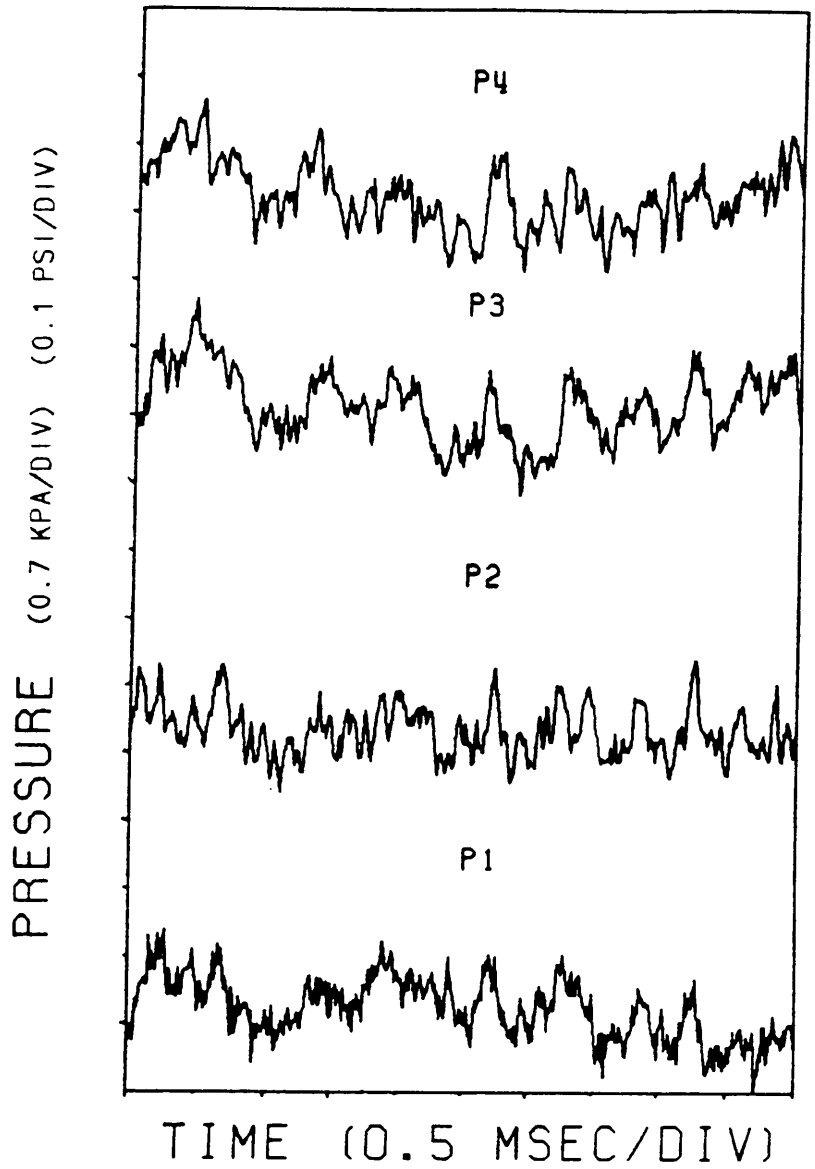

Figure 3. Angle Probe Raw Data: Typical data showing pressure versus time as measured from the high frequency angle probe in the test section.

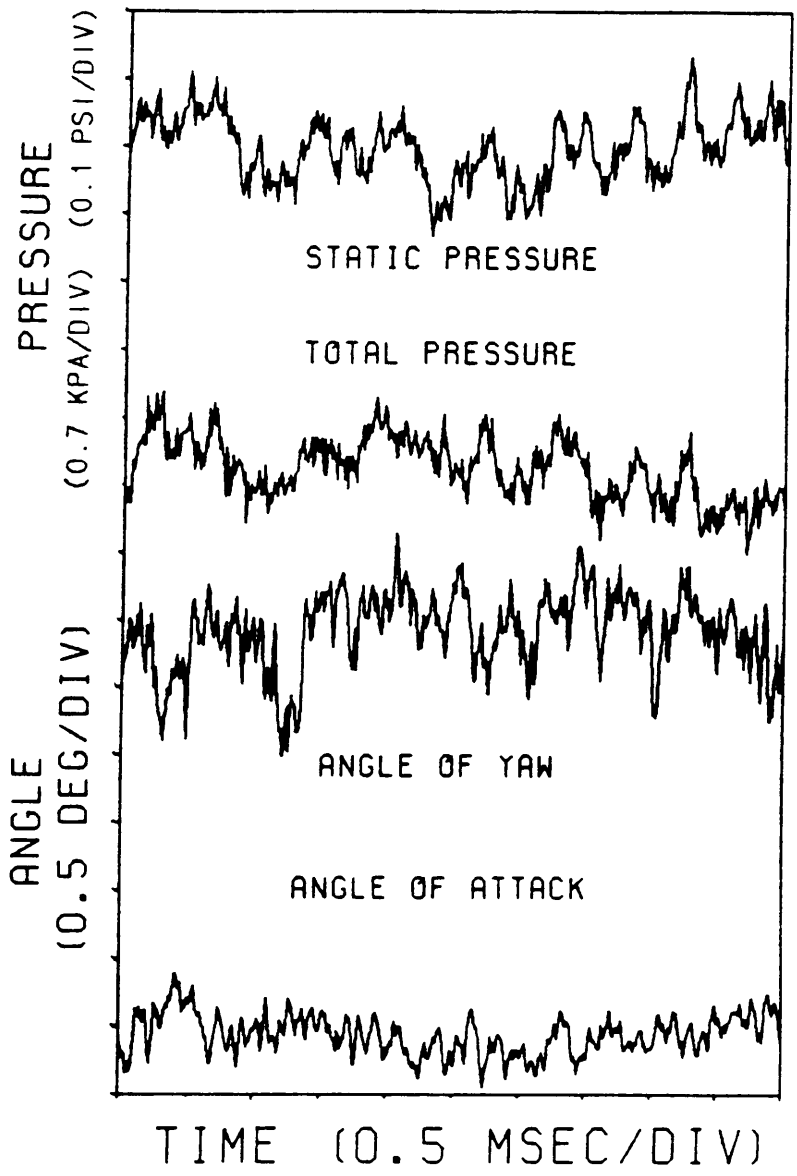

Figure 4. Angle Probe Reduced Data: The data of Fig. 3, interpreted as static pressure, total pressure, and flow angles.

From previous measurements made with the combination probe, it was found that the errors in the measurements of the static pressure, total pressure, and total temperature are $\pm$ 0.34 kPa (0.05 psi), $\pm$ 0.34 kPa (0.05 psi), and $\pm$ 0.12 K (0.2 R), respectively. An error analysis on the quantities calculated from these three measurements is done in Appendix A. The results of the analysis for the maximum normalized errors are presented in Table 1. Each quantity is normalized by the mean value of that quantity. The normalized errors for the Mach number, the velocity, and the mass flux, all have a maximum value of 3.0%. The maximum normalized errors for the static temperature and the density are 0.2% and 0.5%, respectively.

Because of the amount of data taken, it is not feasible to present all the data individually as in Figs. 3 and 4. A summarized figure showing the root-mean-square (rms) value of the turbulence intensity as a function of unit Reynolds number for different Mach numbers is preferable. The error in each rms value is less than 2% of the value, as outlined in Appendix B. In examining the rms figures which follow, it is important to realize that a particular Reynolds number in the tunnel can be achieved by various combinations of total pressure and temperature. Data which appear to be at the same Reynolds number do not correspond to identical tunnel conditions.

Figure 5 shows the rms of the fluctuating total temperature in the settling chamber as measured from the aspirating probe. The data are normalized by the mean total temperature in the tunnel. The rms values are all given in percent. It can be seen that the normalized fluctuating total temperature is not a strong function of Reynolds number or Mach number. For most of the operating envelope of the tunnel, the

Table 1. Individual Quantity Errors

CALCULATED QUANTITY	NORMALIZED ERROR *
MACH NUMBER	3.0%
STATIC TEMPERATURE	0.2%
VELOCITY	3.0%
DENSITY	0.5%
MASS FLUX	3.0%

*Normalized by the mean of the quantity

turbulence intensity is close to 0.2% in terms of normalized total temperature fluctuation.

Figure 6 is the corresponding temperature data measured from the aspirating probe in the test section. Here, a slight Mach number dependency is seen. The normalized rms total temperature fluctuation increases from 0.05% at M = 0.30 to approximately 0.2% at M = 0.70. The data do not show any Reynolds number dependency.

Comparing Figs. 5 and 6, a large difference in the number of data is noticed. This is due to hot wire breakage for the aspirating probe in the test section, and the omission of the data due to periodic disturbances. Further comparison of Figs. 5 and 6 reveals that the level of turbulence, as measured by the normalized rms total temperature fluctuation, does not change between the settling chamber and the test section. Most of the data falls close to the value of 0.2%.

Figure 7 is the rms of the fluctuating total pressure in the settling chamber, normalized by the mean total pressure in the tunnel. It can be seen that the rms value of the total pressure in the settling chamber is independent of Reynolds number, but that it increases with increasing Mach number. At M = 0.30, the average rms fluctuation is about 0.02%. This increases by almost an order of magnitude to 0.15% at M = 0.85. Nevertheless the fluctuating total pressure in the settling chamber is still fairly small for the entire operating envelope of the tunnel.

Figure 8 is the corresponding fluctuating total pressure in the test section, as measured by the angle probe. The maximum rms fluctuation of the total pressure in the test section is about 0.3%. The trend is similar to the normalized total pressure fluctuations in the settling chamber in that both are increasing with Mach number.

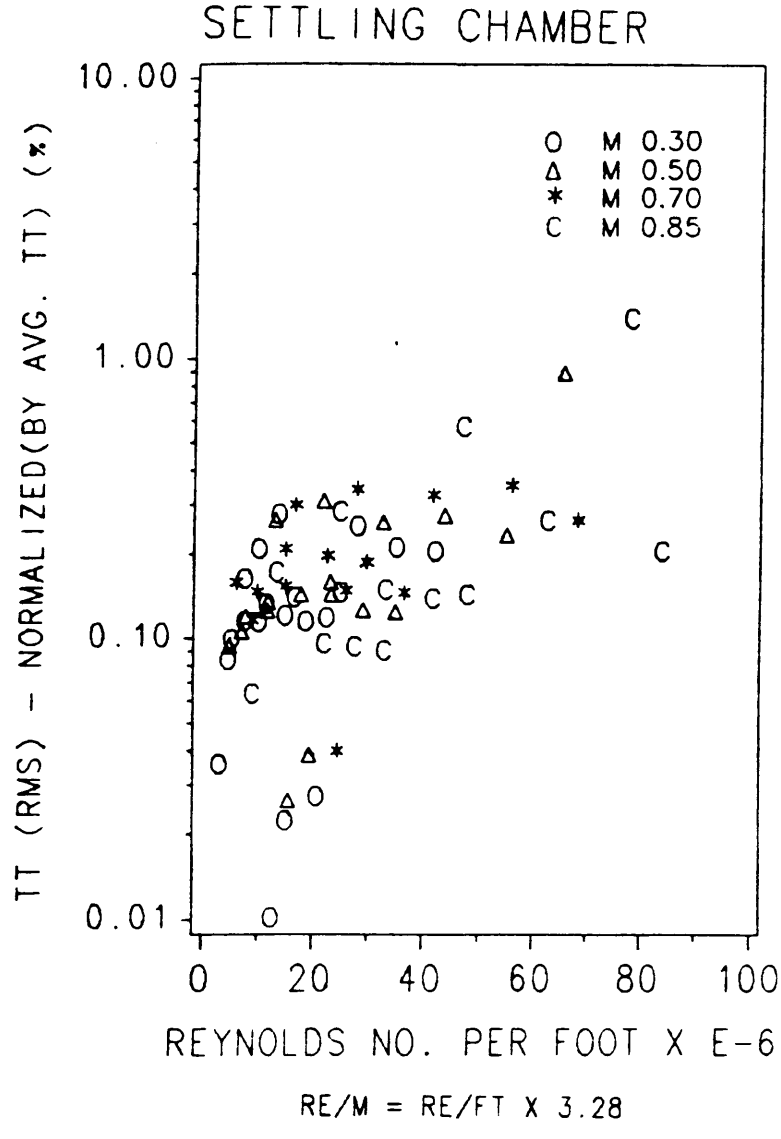

Figure 5. Settling Chamber Total Temperature Fluctuation: Total temperature fluctuation in the settling chamber as measured from the aspirating probe.

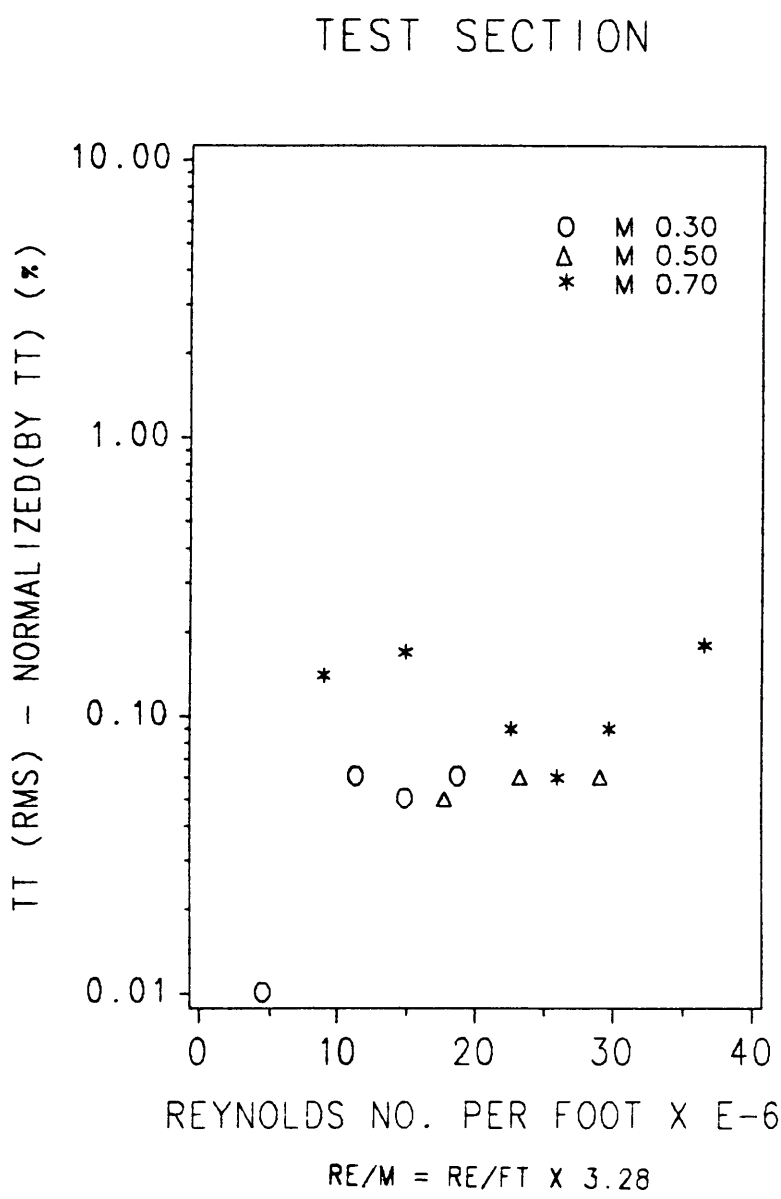

Figure 6. Test Section Total Temperature Fluctuation: Total temperature fluctuation in the test section as measured from the aspirating probe.

The amplitude of the fluctuation is rather independent of Reynolds number. As the Mach number increases from 0.30 to 0.85, the rms value increases from 0.03% to about 0.3%. In general, by comparing Figs. 7 and 8, the rms value of the total pressure is about two times higher in the test section than it is in the settling chamber. The reason for the increase might be the acceleration of the flow from the settling chamber to the test section.

The frequency content of the pressure fluctuation measured in the settling chamber and in the test section is also examined. Typical fast Fourier transforms (FFT) of the fluctuating total pressure data are shown in Fig. 9. From the FFT of the fluctuating total pressure in the settling chamber, a distinct peak can be seen at 462 Hz. This corresponds to the blade passing frequency of the driving fan of the tunnel. In the test section, that distinct frequency can no longer be identified. Instead, the peak seems to be redistributed. Some of the harmonics of the blade passing frequency are, however, still present in the test section.

Figure 10 is the result of flow angularity measurements made with the angle probe. The flow angle fluctuation in the plane parallel to the tunnel side walls is presented. For convenience this is referred to as the angle of attack. Flow angle fluctuation in a plane perpendicular to this plane (angle of yaw) shows the same trend and hence is not presented. All of the data fall below a level of 0.4 degrees.

The fluctuating Mach number, normalized by the local mean Mach number in the test section, is plotted against unit Reynolds number in Fig. 11. The normalized fluctuating Mach number decreases with increasing Mach number. This may be due to the choice of the local mean Mach number in the test section as the normalizing factor. At M = 0.85, the normalized rms fluctuation is about 0.4%. At M = 0.30, it

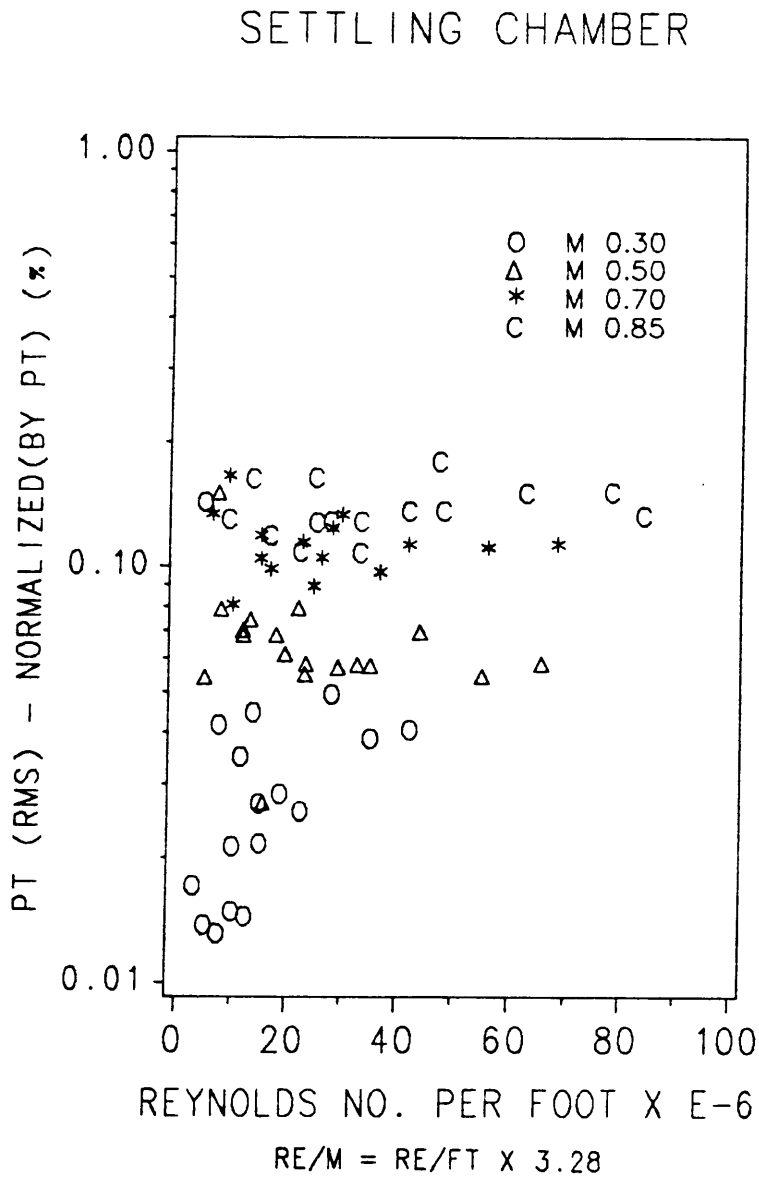

Figure 7. Settling Chamber Total Pressure Fluctuation: Total pressure fluctuation in the settling chamber as measured from the impact probe.

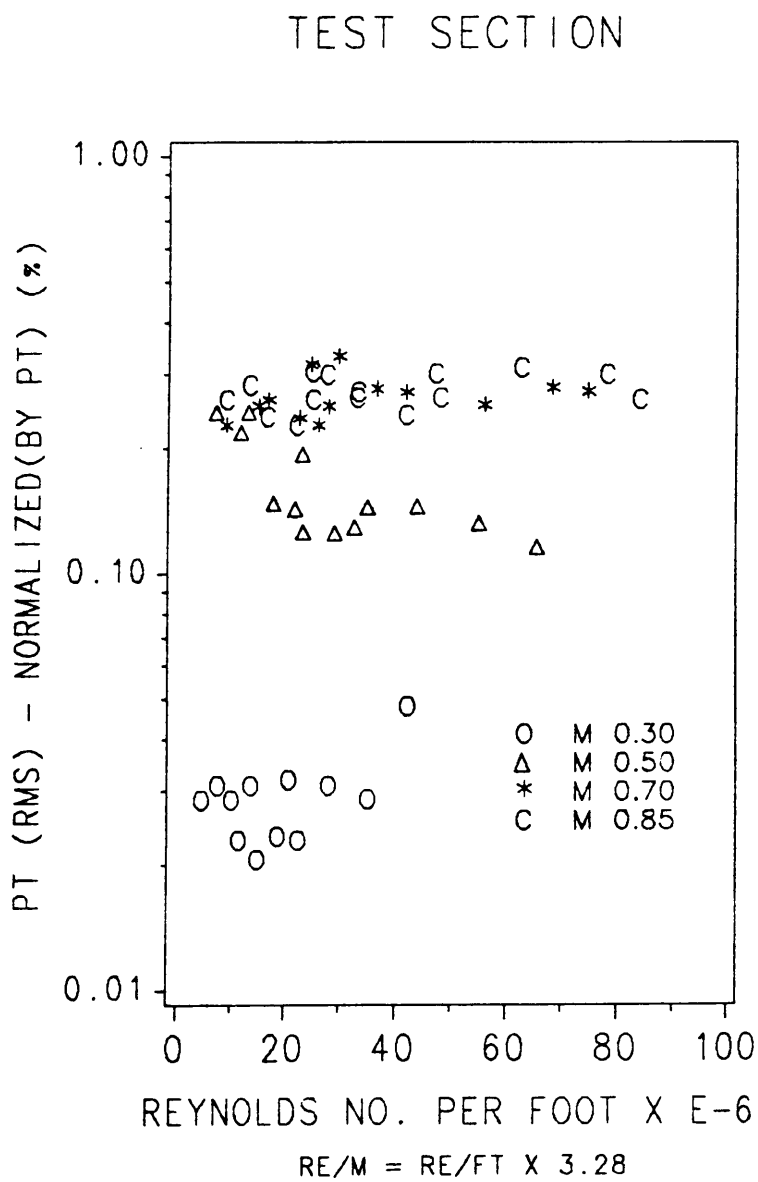

Figure 8. Test Section Total Pressure Fluctuation: Total pressure fluctuation in the test section as measured from the angle probe.

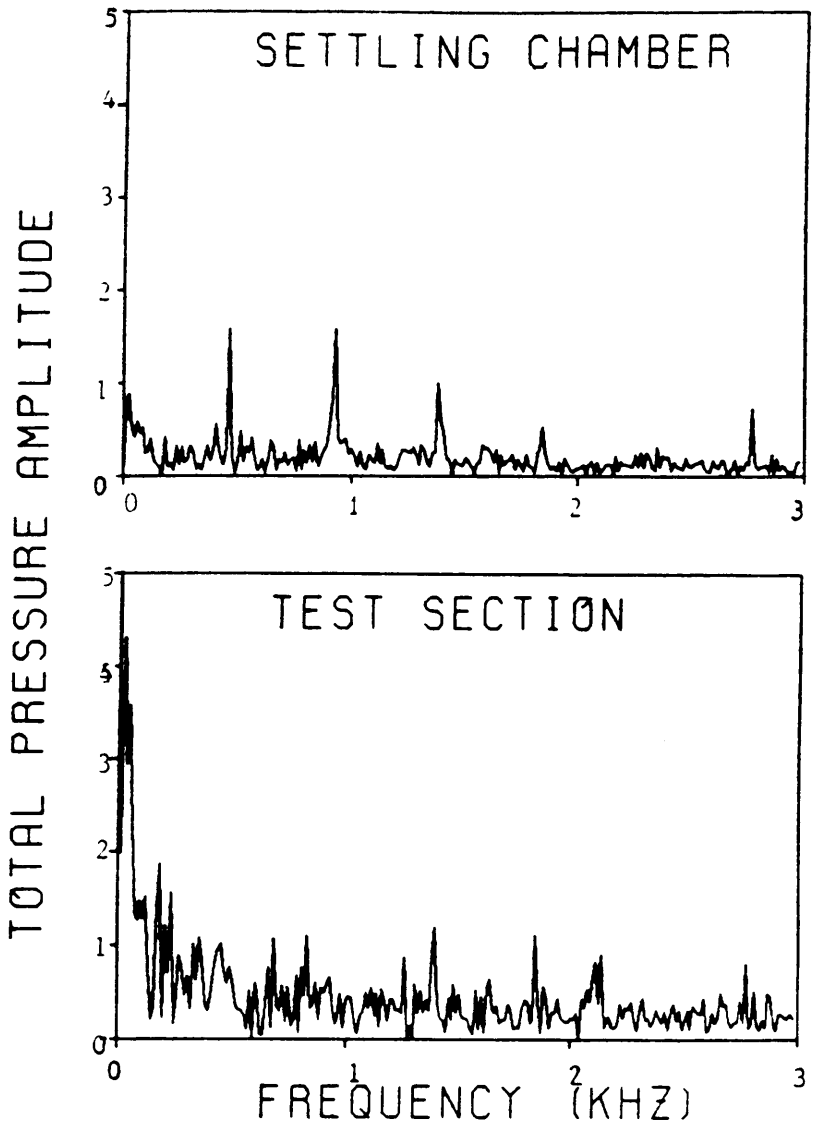

Figure 9. Total Pressure Frequency Spectra: Typical spectra for total pressure fluctuations measured in the settling chamber and test section.

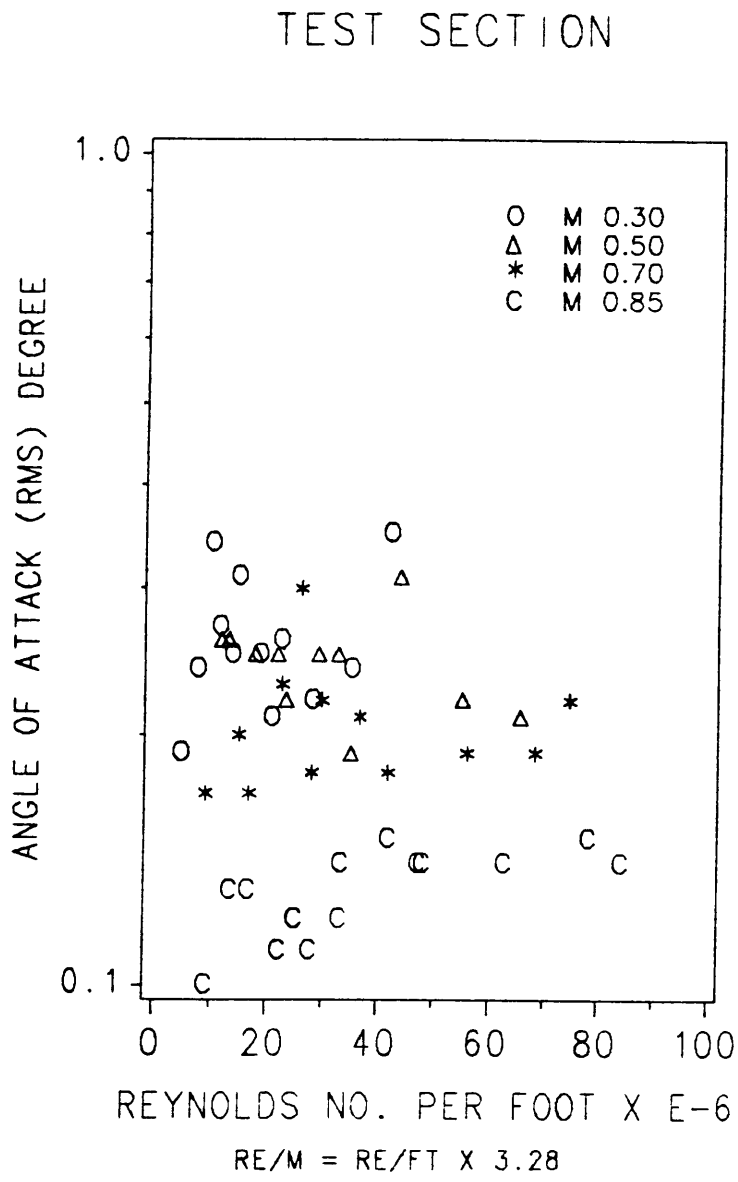

Figure 10. Test Section Flow Angle Fluctuation: Flow angle fluctuation in the test section as measured from the angle probe.

increases to 2.0%. However, in most cases, the normalized Mach number fluctuation is less than 1.0%.

All of the quantities presented thus far have come from separate measurements made by the aspirating and angle probes. The quantities which are presented next fall into the second group of turbulence data. That is, all of the quantities are calculated by combining measurements from the angle probe and aspirating probe.

The first quantity calculated from the measurements of the aspirating probe and the angle probe is the static temperature. Figure 12 is the rms of the fluctuating static temperature in the test section, normalized by the mean static temperature in the test section. The rms fluctuations increase with increasing Mach number. At M = 0.30, the normalized static temperature fluctuation is about 0.05%. The value increases to 0.2% at M = 0.70. Most of the normalized static temperature fluctuations in the test section, however, are close to a value of 0.1%.

With the static temperature and Mach number data known, the velocity data can be calculated. It is well known that velocity fluctuations are of primary and fundamental interest in the determination of disturbance levels in wind tunnels. Figure 13 is the rms of the fluctuating freestream velocity in the test section, normalized by the mean freestream velocity. Once again, the turbulence levels increase with increasing Mach number. At M = 0.30, the rms of the fluctuating velocity has a value of 0.35%. At M = 0.70, the value has increased to approximately 0.6%. With the exception of one data point, the turbulence intensity, in terms of the normalized velocity fluctuations, is less than 0.7%.

The mass flux is the last quantity presented which is calculated from the measurements of the angle and aspirating probes. The rms of the mass flux (ρu) fluctuations in the test section, normalized by the average mass flux, are presented in Fig. 14. It can be seen that the data have no discernable Reynolds or Mach number dependency. All of the mass flux fluctuations, when normalized by the mean mass flux, fall below a value of about 0.5%.

4.2 Periodic Disturbances

As mentioned previously, several tunnel conditions invoked periodic disturbances in the test section. The idea, as outlined in the introduction, that the porous side walls in the test section are the origin of these disturbances, will be discussed in more detail later. Again, these periodic data were not presented in the preceding figures. Also, at M = 0.50 and for unit Reynolds numbers less than 65.6 x 10^6/m (20 x 10^6 /ft), the periodic disturbances become unusually high. This was further investigated during the experiment.

Figure 15 shows the pressure measurements from the angle probe for one of these data points. Only P_1 and P_2 are shown, P_3 and P_4 exhibit similar behavior. The data show a strong periodicity, and all four transducers on the angle probe see the same disturbance. The magnitude of the disturbance is about the same for all four transducers. A fast Fourier transform of the pressure from P_1 is shown in Fig. 16. A distinct peak is seen at 1306 Hz. At this particular tunnel operating condition, the driving fan blade passing frequency was 702 Hz. This can hardly be identified in Fig. 16. The wall static pressure in the test section as measured from a semiconductor

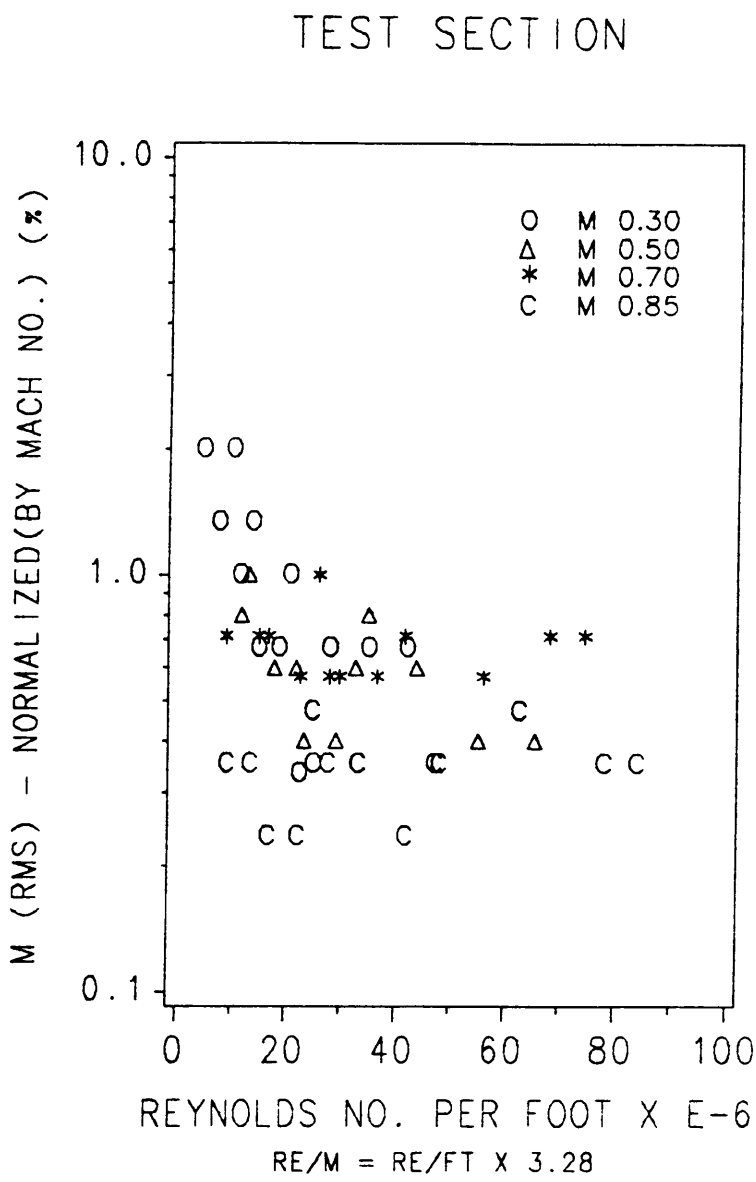

Figure 11. Test Section Mach Number Fluctuation: Mach number fluctuation in the test section as calculated from the measurements of the angle probe.

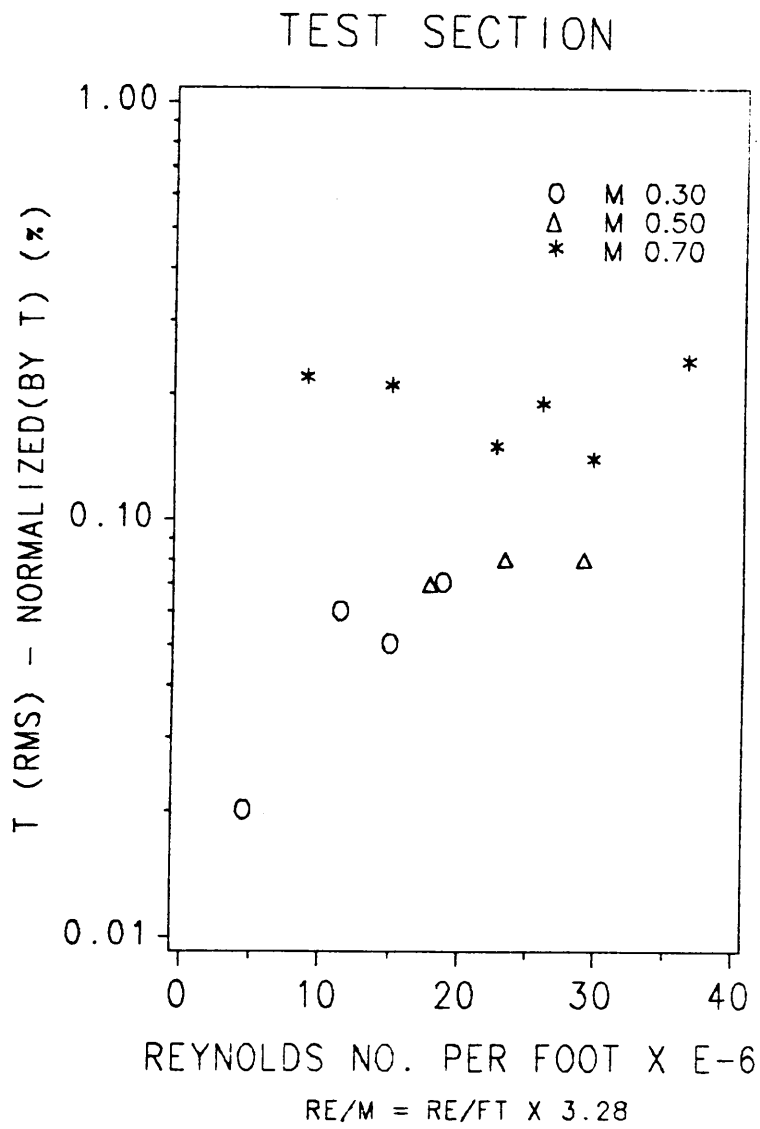

Figure 12. Test Section Static Temperature Fluctuation: Static temperature fluctuation in the test section as calculated from the measurements of the angle probe and the aspirating probe.

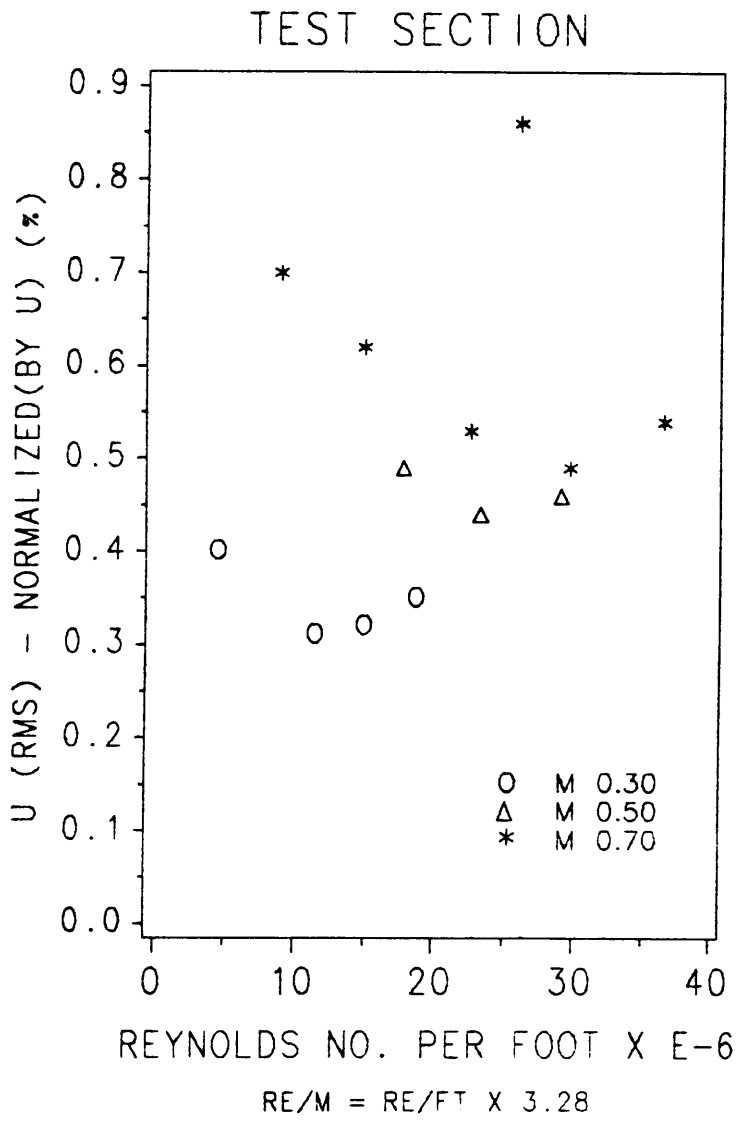

Figure 13. Test Section Velocity Fluctuation: Velocity fluctuation in the test section as calculated from the measurements of the angle probe and the aspirating probe.

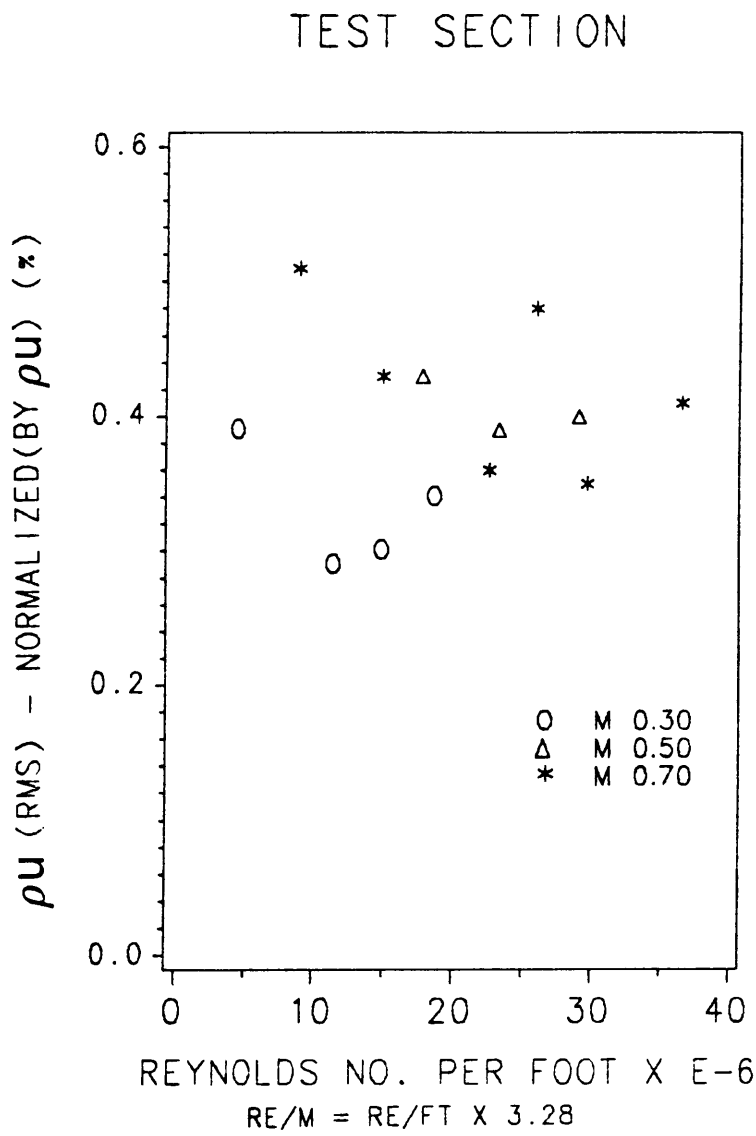

Figure 14. Test Section Mass Flux Fluctuation: Mass flux fluctuation in the test section as calculated from the measurements of the angle probe and the aspirating probe.

pressure transducer flush-mounted on the tunnel side wall is plotted in Fig 17. The corresponding FFT of the signal is shown in Fig 18. Although the periodicity in the wall static pressure measurement is not as pronounced as the angle probe, the same 1306 Hz disturbance is still easily identified from the FFT shown in Fig 18. This leads to the conclusion that the periodic disturbance seen by the angle probe is not due to probe vibration, but is most likely from the tunnel. Careful consideration of Fig. 18 also reveals that, with the exception of the peaks due to periodicity, the side wall static pressure turbulence intensities exponentially decrease as the frequency increases. Comparison with Fig. 9 reveals that this is also true of the total pressure turbulence intensities in the freestream of the test section.

At the end of the experiments in the tunnel, the natural frequency characteristics of the probe stem and support rake were examined. A series of tests were conducted in which an accelerometer was mounted near the tip of the combination probe. With no flow in the tunnel, the probe rake was mechanically vibrated and the frequency spectra from the accelerometer and the pressure transducers on the probe tip were examined. Except for a small peak at around 250 Hz, no distinct peak was found in the spectra. This further confirms that the periodic disturbance seen during the experiment is from the tunnel and is not due to probe vibration. In the next chapter, the possibility of the porous side walls in the test section as the source of the periodic disturbances will be discussed in detail.

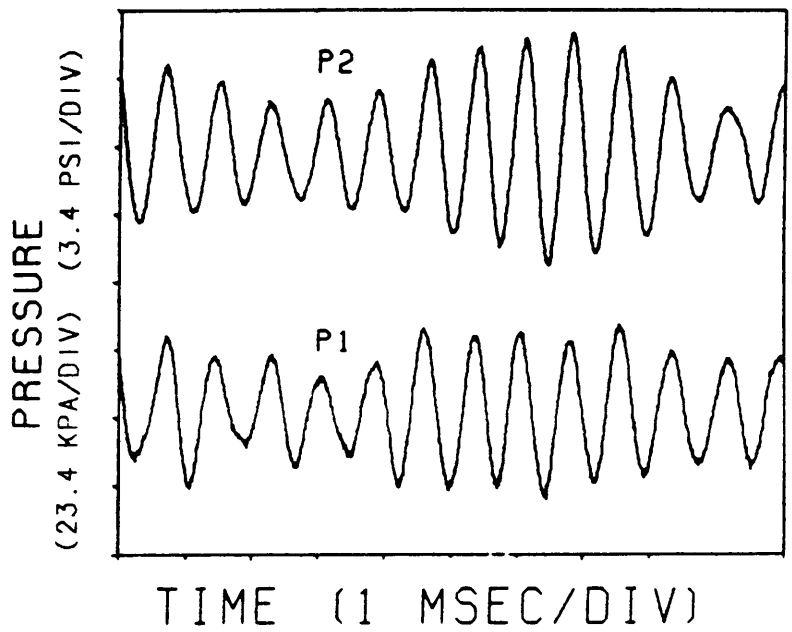

Figure 15. Periodic Pressure Measurements in the Freestream: Pressures measured from the angle probe showing periodic disturbance in the tunnel test section.

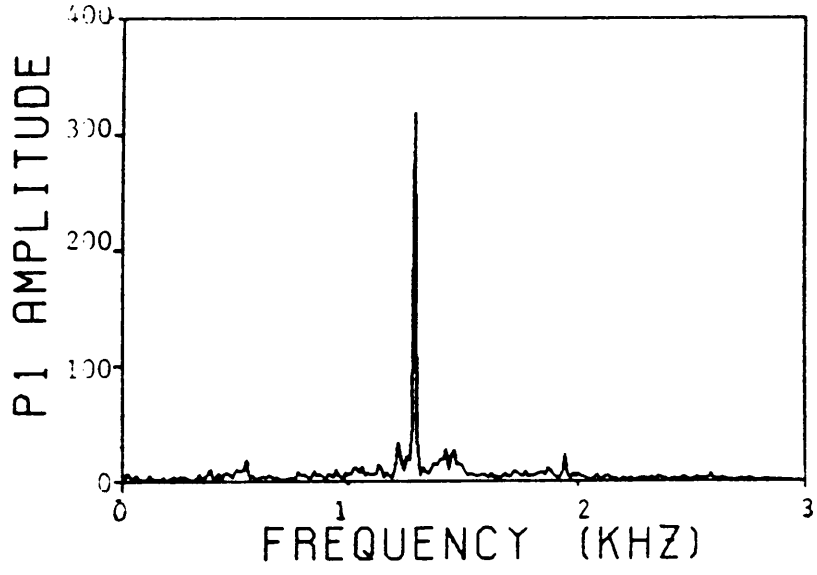

Figure 16. Frequency Spectrum of a Freestream Periodic Disturbance: Spectrum of the data in Fig. 15.

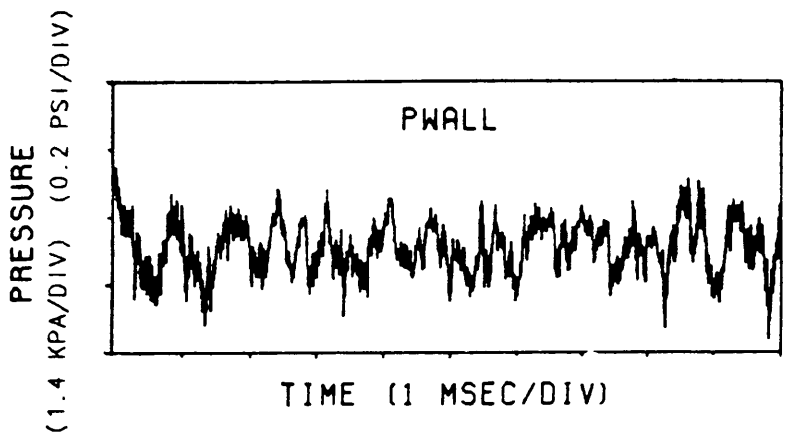

Figure 17. Periodic Pressure Measurement on the Side Wall: Pressure measured from test section side wall showing a periodic disturbance.

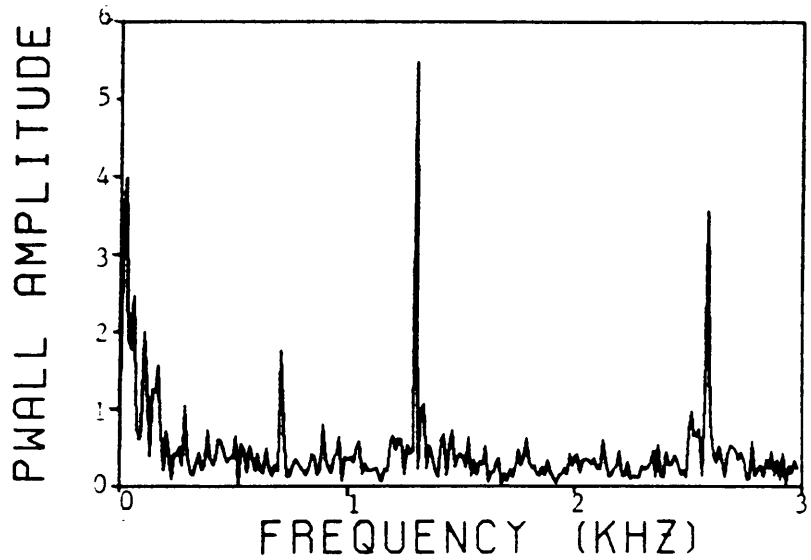

Figure 18. Frequency Spectrum of a Side Wall Periodic Disturbance: Spectrum of the data in Fig. 17.

5.0 Discussion

In this chapter, the acoustic coupling of the test section and plenum chamber via the porous walls is described in more detail as a possible cause of the resonance disturbances observed in the test section. Also, previous turbulence measurements taken in the same tunnel are compared with the present data in this section. Finally, correlation coefficients are calculated in an attempt to determine if one mode of turbulence (vorticity, entropy, or sound) dominates in the tunnel.

5.1 Periodic Disturbances

With the turbulence in the tunnel documented, attention is turned to the periodic disturbances. A source of noise in the test section of a tunnel is thought to be acoustic coupling of the test section and plenum chamber via the perforated side walls. Edge tones are created when vortices are shed by the leading edge of a hole and are reinforced by the sharp trailing edge of the hole (see Fig. 19). The trailing edge vortices propagate back upstream and systematically generate more vortices at the leading edge [10]. The noise generated by the edge tone is radiated into the test section and, because of the periodic nature of the creation of the tones, can induce resonance in the tunnel.

The resonance frequencies created by porous walls have been successfully predicted for tunnels with rectangular test sections [13]. A sketch of the test section and plenum chamber of the 0.3-m TCT is shown in Fig. 20. The porous side walls are 0.18 m (7 in.) high and 0.36 m (14 in.) long and are located upstream of the position where a model would be placed. In Ref. [13], a velocity potential analysis is done on the test section and plenum chamber of a tunnel with perforated side walls. The boundary condition at the perforated wall is that of mass continuity. In addition, an equation for the pressure drop across the perforated wall is developed in terms of the velocity potentials in the test section and plenum chamber. The boundary condition at the outer walls of the plenum chamber is that the normal velocity is zero. With these boundary conditions, the velocity potentials can be solved (see Ref. [13] for details). The resulting eigenvalue equation is

$$\tan p - \left(\frac{\beta^2}{R}\right)\cot(Rdp) + \left(2\beta^2 k \frac{T}{H}\right)p = 0 \qquad (6.1)$$

$$\textit{where}\quad R = \sqrt{(1 - M^2) - \frac{M^2}{1 - M^2}}$$

$$\beta = \sqrt{1 - M^2}$$

$$T = 0.85D + Z$$

D = hole diameter

Z = plate thickness

$$k = \frac{1 - \sigma}{\sigma}$$

σ = open-area ratio

From this equation, it can be seen that the eigenvalues p are functions of the Mach number M, the ratio of plenum chamber depth to tunnel depth d, the effective hole diameter of the perforations T, an open-area-ratio function k, and the tunnel depth H. The eigenvalues p are in turn a function of the resonance frequency [13].

$$p = \frac{\pi f H}{a\beta} \tag{6.2}$$

where f = the resonance frequency

and a = the speed of sound

Thus for a given Mach number, the resonance frequency due to acoustic coupling of the test section and the plenum chamber can be calculated for a given geometry (see Appendix C for details of the calculation for the 0.3-m TCT). This was done for a tunnel condition of T_T = 250 K (450 R) and the result presented in Fig. 21.

The modes in Fig. 21 correspond to the first, third, and fifth solutions of the above equation for the eigenvalues p. The second and fourth solutions of the equation have no meaning as they are the solutions at points where eigenvalue equation is undefined. The predicted frequencies from the acoustic coupling theory were calculated, as outlined above, by varying the Mach number from 0.0 to 1.0. It can be seen in Fig. 21 that the resonance frequencies observed during the experiment agree relatively well with the theory. This would suggest that acoustic coupling of the test section and the plenum chamber via the perforated side walls is indeed a source of resonance in the tunnel.

Equation 6.1 also reveals that for a given tunnel, the eigenvalues p are a function of the Mach number only. Then for a given Mach number, equation 6.2 reveals that the

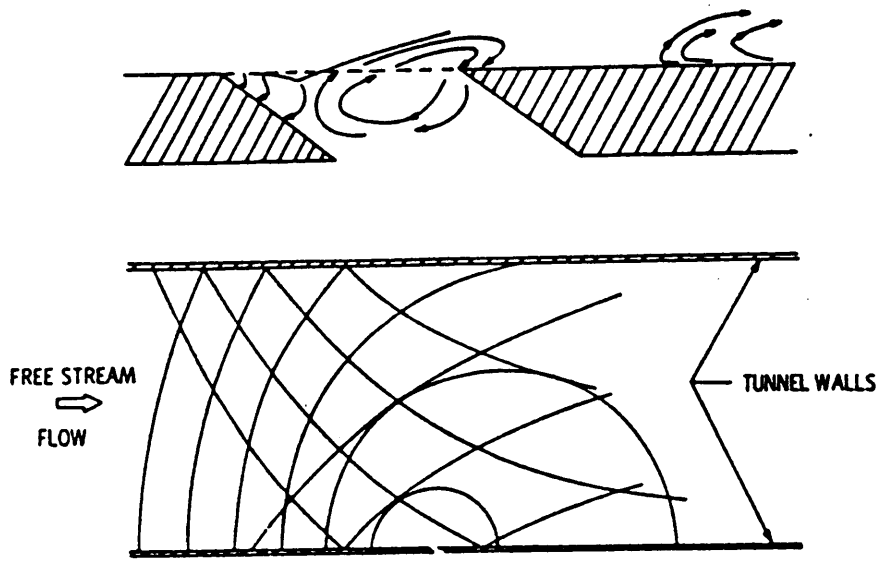

Figure 19. Edge Tone Noise Source and Radiation: (From Ref. [10])

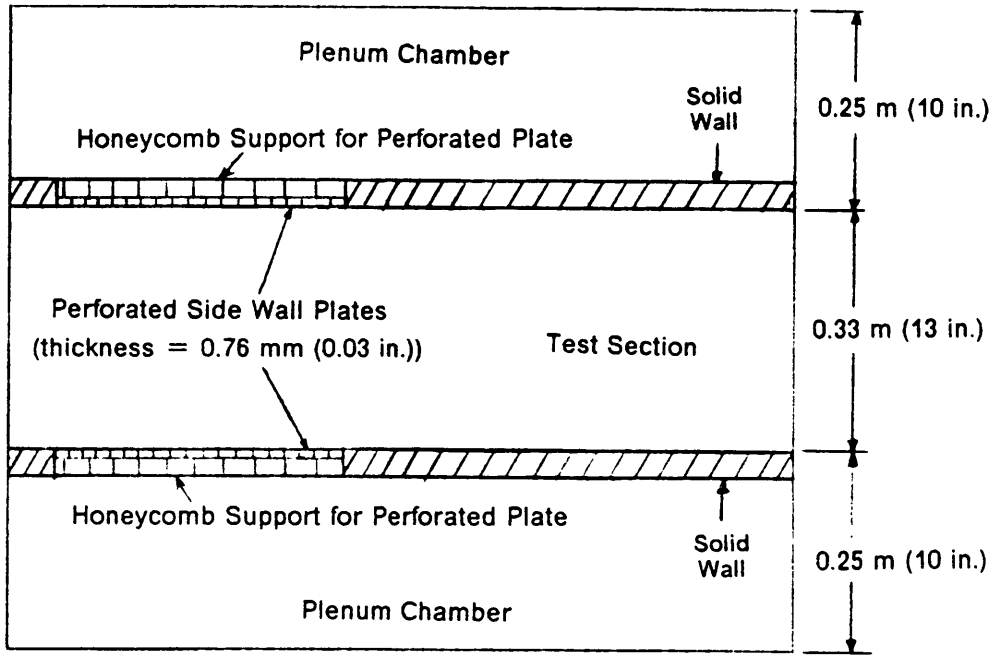

Figure 20. 0.3m-TCT Test Section and Plenum Chamber

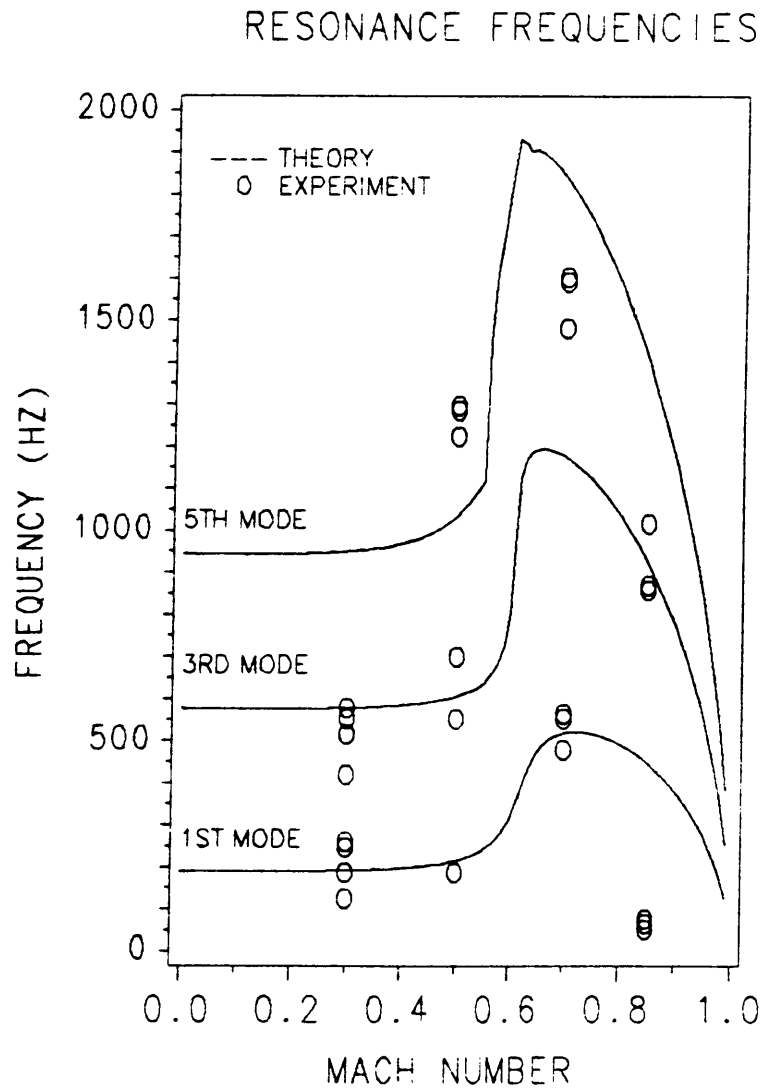

Figure 21. Mach Number Dependency of Resonance Frequencies: Theory lines represent predicted resonance frequencies due to acoustic coupling of the test section and plenum chamber.

resonance frequency f is only a function of the speed of sound a. Thus, the natural frequency at one temperature should be related to the natural frequency at another temperature by a direct ratio of the speeds of sound. That is,

$$\frac{f_{T_1}}{f_{T_2}} = \frac{a_{T_1}}{a_{T_2}} \tag{6.3}$$

where f_{T_1} and a_{T_1} are the natural frequency and speed of sound, respectively, at a temperature of T_1, and f_{T_2} and a_{T_2} are the natural frequency and speed of sound at a temperature of T_2. Equation 6.3 was used to calculate the expected frequencies at a total temperature of 185 K (333 R) from the observed frequencies at 250 K (450 R). The result for M = 0.5, the condition at which the largest resonance disturbances are found, is presented in Table 2. The calculated frequencies and observed frequencies at a tunnel total temperature of 185 K (333 R) match almost exactly. This further supports the idea that the resonance disturbances are caused by acoustic coupling of the test section and plenum chamber via the perforated side walls.

The acoustic coupling theory, however, cannot explain all of the data. For instance, at T_T = 120 K (216 R), there were no observed natural frequencies. If the disturbances were acoustic in nature, there should have been periodic disturbances occurring at frequencies calculated with equation 6.3. Instead, there were no periodic disturbances at all. Also, the magnitude of the resonance disturbances at a total temperature of 185 K (333 R) were considerably smaller than the disturbances at a total temperature of 250 K (450 R). This cannot be explained by the acoustic coupling theory. A possible explanation for the decreasing disturbances might be that the resonance is coupled with the tunnel stiffness such that as the tunnel temperature decreases, the resonance dissipates. This may also explain the lack of resonance

Table 2. Calculated and Observed Resonance Frequencies

MACH NUMBER = 0.50			
TOTAL PRESSURE (atm)	T = 250 K (450 R) MEASURED FREQUENCY (Hz)	T = 185 K (333 R) * CALCULATED FREQUENCY (Hz)	T = 185 K (333 R) MEASURED FREQUENCY (Hz)
1.2	1221	1050	1038
2.0	1221	1050	1062
3.0	1282	1103	1100
4.0	1294	1113	1111
5.0	1294	1113	1111

* Calculated with equation 6.3

at 120 K (216 R). That is, at 120 K (216 R), the resonance disturbances might be so small that they cannot be measured.

If the periodic disturbances are caused by the acoustic coupling of the test section and the plenum chamber, another possible explanation for the lack of disturbances at a total temperature of 120 K (216 R) might be that the holes in the side walls became plugged. This would be possible if the tunnel were not slowly brought to its operating condition of 120 K (216 R). If the total temperature dropped below, and was then brought back up to 120 K (216R), nitrogen droplets could have formed. These droplets could then have plugged the holes, and thus eliminated the acoustic coupling of the test section and the plenum chamber.

Without further experimentation, it can only be postulated that the acoustic coupling of the test section and plenum chamber via the perforated side walls seems to be a plausible explanation for the periodic disturbances observed in the test section.

5.2 *Comparison with Previous Measurements*

Before comparing the present turbulence data with previous measurements in the 0.3-m TCT, it is important to point out some of the modifications made to the tunnel recently [16]. The current tunnel has a new test section with top and bottom adaptive walls and became operational in May 1986. No modification was made in the settling chamber. The size of the test section is now 0.33 m x 0.33 m (13 in. x 13 in.) and has a contraction ratio of 10.7 relative to the settling chamber. All other turbulence measurements in the tunnel that appear in literature were taken before the adaptive wall test section was installed. The previous test section was 0.2 m x 0.61 m (8 in. x

24 in.) and had a contraction ratio of 9.4. Thus the present test section has an increase in the contraction ratio of 14% compared to the previous test section. This should help in reducing the turbulence intensities. Perhaps more important is the replacement of the high-speed diffuser downstream of the test section. It was found that the previous diffuser had separated boundary layers and generated more noise in the tunnel. The newly installed diffuser is longer and has a shallower angle to prevent separation. To accommodate the longer diffuser, the overall tunnel length was increased by 8 feet. The higher contraction ratio and the longer diffuser should decrease the turbulence intensities in the test section.

Fluctuating pressure in the settling chamber was also measured by Johnson and Stainback [17]. A commercially available pressure transducer designed to operate at cryogenic temperatures was used. The transducer was mounted flush to the inside surface of the settling chamber. Although this is different from the present arrangement, (the pressure transducer was mounted in an impact probe pointing upstream), the local mean velocity in the settling chamber is so small that the wall static pressure and the impact probe pressure are essentially indistinguishable. In Ref. [17] it was found that the levels of pressure fluctuations increase with increasing Mach number, which is consistent with the present investigation. The maximum normalized pressure fluctuation in the settling chamber was about 0.2% at a test section Mach number of 0.80 (Ref. [17]). In the present experiment, the maximum normalized pressure fluctuation is 0.2% at $M = 0.85$. The agreement between the data is not surprising, since there is no change made in the settling chamber and the measuring instruments are similar in both experiments. In addition, power spectra of the fluctuating pressure in Ref. [17] also show discrete frequencies due to the fan

blade passing frequency and its harmonics. This again agrees well with the present experimental observation.

In other experiments, Stainback and Johnson [6] measured quantities in both the settling chamber and the test section, as done in the present case. The data in Ref. [6] indicate the maximum normalized pressure fluctuations increase from 0.15% in the settling chamber to 0.3% in the freestream of the test section. The increase in turbulence intensities as the flow accelerates from the settling chamber to the test section is consistent with the present experiment. The magnitude of the fluctuations in both the settling chamber and the test section agree with the magnitudes found in the current experiment. Recall that in the present case, the maximum normalized pressure fluctuations increase from 0.15% in the settling chamber to 0.3% in the freestream of the test section.

Freestream velocity fluctuations in the test section were also measured by Stainback and Johnson in Ref. [6], using a three-wire hot-wire probe. The maximum normalized value was found to be 7.5% at M = 0.70. In the present experiment, the maximum normalized fluctuation is 0.7% at M = 0.70. The value measured in Ref. [6] is much higher, an order of magnitude higher, than the value in the present case. This might be caused by the use of a three-wire hot-wire probe in Ref. [6]. Probes of this nature tend to measure turbulence intensities much higher than expected [18].

5.3 *Correlation Coefficients*

Correlation coefficients have been used in the past to to determine the major source of random turbulence in a tunnel [19]. The velocity and density correlation coefficient

$R_{u\rho}$, the velocity and total temperature correlation coefficient R_{uT_T}, and the density and total temperature correlation coefficient $R_{\rho T_T}$ are defined as follows:

$$R_{u\rho} = \frac{\overline{u'\rho'}}{\tilde{u}\tilde{\rho}}$$

$$R_{uT_T} = \frac{\overline{u'T_T'}}{\tilde{u}\tilde{T}_T}$$

$$R_{\rho T_T} = \frac{\overline{\rho'T_T'}}{\tilde{\rho}\tilde{T}_T}$$

where a primed quantity represents an instantaneous measurement of that quantity, a bar represents the mean of a quantity, and a quantity with a tilde is the rms value of that quantity. In Ref. [19], small perturbations are applied to the equation of state as well as to the conservation of momentum, the conservation of energy, and the conservation of mass. The resulting equations are linearized and used to define three modes of fluctuation: vorticity, entropy, and sound-wave. Reference [20] then relates small perturbations in velocity, density, and total temperature to fluctuations due to vorticity, entropy, and sound, as defined in Ref. [19]. Thus, if it is assumed that only one mode of turbulence is present, the fluctuations of velocity, density, and total temperature can be described in terms of fluctuations due to vorticity, entropy, or sound. The resulting equations can then be substituted into the definitions of the correlation coefficients. In Ref. [18], this substitution was performed and it was found that the correlation coefficients have specific values if it is assumed that the turbulence is due to a single mode. These specific values were calculated in Ref. [18], and the results are presented in Table 3. Correlation coefficients can be calculated for the data in an experiment using the definitions given above. The

calculated coefficients can then be compared with Table 3 to see if one mode of turbulence dominates in the tunnel. For example, if the data resulted in calculated values of 0, 1, and 0 for $R_{u\rho}$, R_{uT_T}, and $R_{\rho T_T}$ respectively, then the major mode of turbulence would be vorticity. If the data resulted in calculated values of -1, -1, and 1 for $R_{u\rho}$, R_{uT_T}, and $R_{\rho T_T}$ respectively, then the major mode of turbulence would be upstream moving sound, and so forth.

All of the correlation coefficients were calculated for the data in the present experiment to see if a major mode of turbulence could be determined. Figures 22, 23, and 24 show the correlation coefficients for various Mach numbers plotted against Reynolds number. Figure 23 suggests that entropy is the major mode of turbulence since the values of R_{uT_T} center around 0. However, if entropy was the major mode of turbulence, $R_{u\rho}$ should have a value of 0, and $R_{\rho T_T}$ should have a value of -1, as shown in Table 2. Figures 22 and 24 reveal that this is not the case. These correlation coefficients do not center around any particular values. Therefore, it does not appear that one mode of turbulence dominates in the tunnel. The turbulence in the tunnel seems to be caused by all three fundamental modes: vorticity, entropy, and sound.

Table 3. Correlation Coefficients for Single Mode Disturbances

MODE	R_{up}	R_{uT_T}	$R_{\rho T_T}$
VORTICITY	0	1	0
ENTROPY	0	0	-1
UPSTREAM MOVING SOUND	1	1	1
DOWNSTREAM MOVING SOUND	-1	-1	1

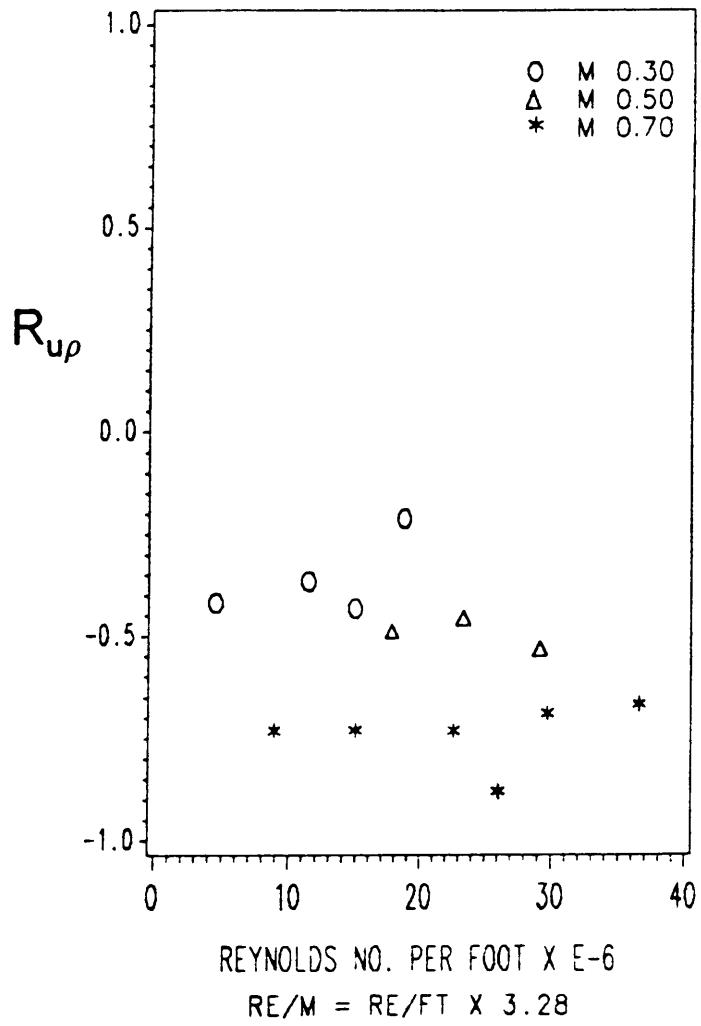

Figure 22. Velocity and Density Correlation Coefficients

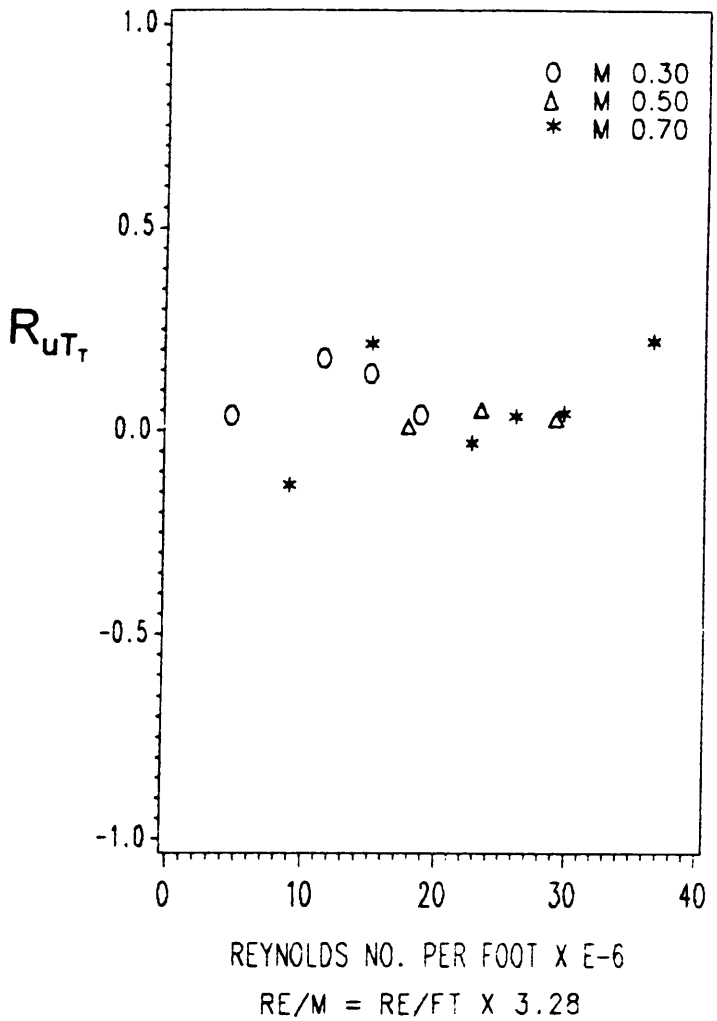

Figure 23. Velocity and Total Temperature Correlation Coefficients

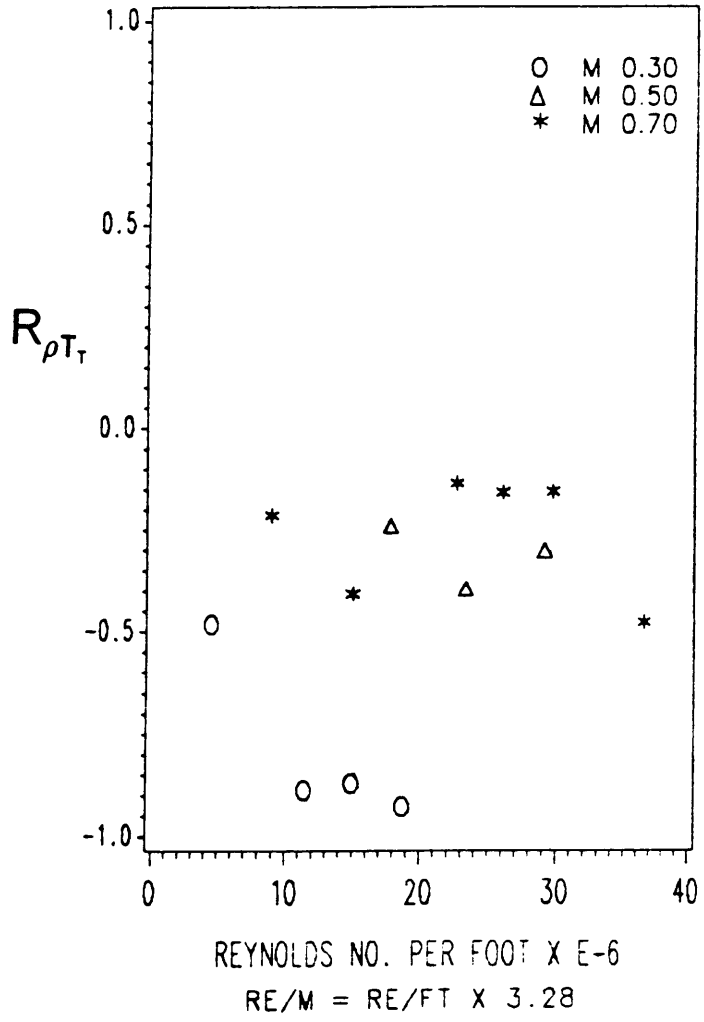

Figure 24. Density and Total Temperature Correlation Coefficients

6.0 Conclusions and Recommendations

A newly developed high-frequency-response combination probe was used to make time-resolved measurements in a high-dynamic pressure, transonic cryogenic wind tunnel. Turbulence measurements were taken in the settling chamber and test section of the 0.3-m TCT at NASA Langley Research Center. Measurements of fluctuating total temperature, total and static pressures, and flow angularity were made in the experiment. From these measurements, fluctuations of Mach number, static temperature, velocity, and mass flux were calculated. It was found that at certain tunnel operating conditions, a large amplitude periodic disturbance is present in the tunnel, which creates unusually high freestream turbulences. However, for all other tunnel operating envelopes, the turbulence intensities are generally small. In the settling chamber as well as in the test section, the normalized rms total temperature fluctuations are about 0.2%. The maximum normalized total pressure fluctuations in the settling chamber are 0.15%, while those in the test section are 0.3%. The normalized rms fluctuations for velocity in the test section are less than 0.7%. Calculated correlation coefficients failed to show vorticity, entropy, or sound as the dominant source of turbulence in the tunnel. It is therefore believed that the three fundamental modes of turbulence coexist in the 0.3-m TCT.

The periodic disturbances in the tunnel are possibly caused by acoustic coupling of the test section and the plenum chamber via the perforated side walls. The resonance frequencies observed agreed well with the frequencies predicted by Mabey's [13] acoustic coupling theory.

It is recommended that further tests be conducted in the 0.3-m TCT to positively identify the source of the periodic disturbances. The perforated side walls could be removed to see if the acoustic coupling theory is valid. Until the origin of the periodicity is positively identified, it is recommended that experiments should not be conducted at operating conditions which invoke tunnel resonance.

Appendix A. Error Analysis on the Absolute Value of Calculated Properties

From previous measurements made with the combination probe, it was found that the errors in the measurements of P, P_T, and T_T are $\pm$ 0.34 kPa (0.05 psi), $\pm$ 0.34 kPa (0.05 psi), and $\pm$ 0.12 K (0.2 R), respectively. Using these values, the error in all of the derived quantities can be calculated using a formula found in Ref. [21].

$$\omega_R = \left[\left(\frac{\partial R}{\partial v_1} \omega_1 \right)^2 + \left(\frac{\partial R}{\partial v_2} \omega_2 \right)^2 + \cdots + \left(\frac{\partial R}{\partial v_n} \omega_n \right)^2 \right]^{1/2}$$

The confidence interval ω_R is for the result R which is calculated with the quantities v_1, v_2, ..., and v_n which have confidence intervals ω_1, ω_2 ,....., and ω_n, respectively. The Mach number equation is

$$M = \sqrt{\left(\frac{2}{\gamma - 1} \right) \left[\left(\frac{P_T}{P} \right)^{\frac{\gamma-1}{\gamma}} - 1 \right]}$$

Substituting M for R, P_T for v_1, P for v_2 , and doing the necessary differentiation yields for the normalized error

$$\frac{\omega_M}{M} = \left[\left(\frac{1}{M^2 P \gamma} \left(\frac{P_T}{P} \right)^{\frac{-1}{\gamma}} \omega_{P_T} \right)^2 + \left(\frac{-1}{M^2 P \gamma} \left(\frac{P_T}{P} \right)^{\frac{\gamma-1}{\gamma}} \omega_P \right)^2 \right]^{1/2}$$

The equation for T is

$$T = T_T\left[1 + \frac{\gamma - 1}{2} M^2\right]^{-1}$$

The normalized error is then

$$\frac{\omega_T}{T} = \left[\left(\frac{\omega_{T_T}}{T_T}\right)^2 + \left[\left(\frac{T}{T_T}\right)(1-\gamma)M\omega_M\right]^2\right]^{1/2}$$

For the velocity

$$u = M\sqrt{\gamma RT}$$

and

$$\frac{\omega_u}{u} = \left[\left(\frac{\omega_M}{M}\right)^2 + \left(\frac{M}{2}\frac{\omega_T}{T}\right)^2\right]^{1/2}$$

Using the ideal gas equation of state, the normalized error for the density is

$$\frac{\omega_\rho}{\rho} = \left[\left(\frac{\omega_P}{P}\right)^2 + \left(\frac{-\omega_T}{T}\right)^2\right]^{1/2}$$

Finally, for the mass flux

$$\frac{\omega_{\rho u}}{\rho u} = \left[\left(\frac{\omega_\rho}{\rho}\right)^2 + \left(\frac{\omega_u}{u}\right)^2\right]^{1/2}$$

The maximum normalized errors for the present experiment were found to be

$$\frac{\omega_M}{M} = 3.0\%$$

$$\frac{\omega_T}{T} = 0.2\%$$

$$\frac{\omega_u}{u} = 3.0\%$$

$$\frac{\omega_\rho}{\rho} = 0.5\%$$

$$\frac{\omega_{\rho u}}{\rho u} = 3.0\%$$

Appendix B. Error Analysis on RMS Values for Fluctuating Properties

Statistical analysis shows that the confidence interval for a rms measurement is a function of the number of measurements taken to calculate the rms value. The error on the individual measurements of the properties does not influence the error of the rms value. Thus, the more measurements taken to calculate the rms value, the more confidence there is in the rms value.

From Ref. [22], a 95% confidence interval on the variance for a large number of data points is

$$\frac{(N-1)s^2}{(N-1)+2\sqrt{2(N-1)}} \leq \sigma^2 \leq \frac{(N-1)s^2}{(N-1)-2\sqrt{2(N-1)}}$$

where

N = number of data points

s^2 = measured variance

σ^2 = actual variance

The variance is the square of the standard deviation, which is the equivalent of a rms value. For the standard deviation, or rms value, the 95% confidence interval for a large number of data points is

$$\sqrt{\frac{(N-1)}{(N-1)+2\sqrt{2(N-1)}}}\,s \leq \sigma \leq \sqrt{\frac{(N-1)}{(N-1)-2\sqrt{2(N-1)}}}\,s$$

s = measured standard deviation (rms value)

σ = actual standard deviation

In the present experiment, almost every rms value was calculated using 8192 data points. Substituting $N = 8192$ into the equation for the standard deviation yields

$$0.98\,s \leq \sigma \leq 1.02\,s$$

Thus the error on each rms value is less than 2% of the value.

$$\text{error} \leq 0.02\ \text{rms}$$

Appendix C. Acoustic Coupling of the Test Section and Plenum Chamber

A velocity potential analysis on the test section and plenum chamber, utilizing mass continuity at the perforated wall, results in the following eigenvalue equations (see Ref. [13] for details)

$$\tan p - \left(\frac{\beta^2}{R}\right)\cot(Rdp) + \left(2\beta^2 k \frac{T}{H}\right)p = 0 \quad 0 \leq M \leq 0.618$$

$$\tan p + \left(\frac{\beta^2}{Q}\right)\cot(Qdp) + \left(2\beta^2 k \frac{T}{H}\right)p = 0 \quad 0.618 \leq M \leq 1.0$$

$$\text{where} \quad R = \sqrt{(1 - M^2) - \frac{M^2}{1 - M^2}}$$

$$\beta = \sqrt{1 - M^2}$$

$$Q^2 = -R^2$$

$$d = \frac{\text{plenum chamber height}}{1/2 \text{ tunnel height}} = 1.538$$

$$\text{plenum chamber height} = 0.25\,m \text{ (10 in.)}$$

$$H = \text{tunnel height} = 0.33\ m\ (13\ \text{in.})$$

$$T = \text{effective hole diameter} = 0.85D + Z = 1.02\ mm\ (0.0402\ \text{in.})$$

$$D = \text{hole diameter} = 0.3\ mm\ (0.012\ \text{in})$$

$$Z = \text{plate thickness} = 0.76\ mm\ (0.030\ \text{in})$$

$$k = \frac{1-\sigma}{\sigma} = 8.09$$

$$\sigma = \text{open-area ratio} = 0.11$$

Thus for a given Mach number M, one can solve the appropriate eigenvalue equation for p. A sensitivity analysis shows that an order of magnitude change in the effective hole diameter T causes a negligible change in the calculated eigenvalues p. The corresponding resonance frequency can be found using an equation in Ref. [13].

$$p = \frac{\pi f H}{a\beta}$$

Where f = the resonance frequency

and a = the speed of sound

The above procedure can be followed for various Mach numbers to produce the expected frequency lines found in Fig. 21. The different modes of natural frequency can be found by using successive real solutions of the eigenvalue equations.

References

1. Jones, L. J., "The Transonic Reynolds Number Problem," NASA CP-2009, presented at a High Reynolds Number Research Workshop at the Langley Research Center, Hampton, VA, October 1976.

2. Lynch, F. T., and Patel, D. R., "Some Important New Instrumentation Needs and Testing Requirements for Testing in a Cryogenic Wind Tunnel Such as the NTF," AIAA-82-0605, Aerodynamic Testing Conference, Williamsburg, VA, March 1982.

3. Varner, M. O., "Noise Generation in Transonic Tunnels," AIAA Journal, Vol. 13, No. 11, November 1975, pp. 1417-1418.

4. Owen, F. K., Stainback, P. C., and Harvey, W. D., "An Evaluation of Factors Affecting the Flow Quality in Wind Tunnels and Testing Techniques," Paper No. 12, AGARD-CP-348, February 1984.

5. Stainback, P. C., Johnson, C. B., and Basnett, C. B., "Preliminary Measurements of Velocity, Density and Total Temperature Fluctuations in Compressible Subsonic Flow," AIAA-83-0384, Aerospace Sciences Meeting, Reno, NV, January 1983.

6. Johnson, C. B., Johnson, W. G., Jr., and Stainback, P. C., "A summary of Reynolds Number Effects on Some Recent Tests in the Langley 0.3-m Transonic Cryogenic Tunnel," SAE-861765, Aerospace Technology Conference and Exposition, Long Beach, CA, October 1986.

7. Ng, W. F., and Rosson, J. C., "Cryogenic Tunnel Measurement of Total Temperature and Pressure," AIAA Journal of Aircraft, Vo., 23, No. 3, March 1986, pp. 244-249.

8. Ng, W. F., Gundappa, M., and Peterson, J. B., Jr., "Turbulence Measurements in a Transonic Cryogenic Wind Tunnel," AIAA-88-2026, Aerodynamic Testing Conference, San Diego, CA, May 1988.

9. Dougherty, N. S., Jr., and Steinle, F. W. Jr., "Transition Reynolds Number Comparisons in Several Major Transonic Tunnels," AIAA-74-627, Aerodynamic Testing Conference, Bethesda, MD, July 1974.

10. Schutzenhofer, L. A., and Howard, P. W., "Suppression of Background Noise in a Transonic Wind-Tunnel Test Section," AIAA Journal, Vol. 13, No. 11, November 1975, pp. 1467-1471.

11. Cox, R. N., and Freestone, M. M., "Design of Ventilated Walls With Special Emphasis on the Aspect of Noise Generation," *Fluid Motion Problems in Wind Tunnel Design*, AGARD Report No. 602, No. 6, November 1972.

12. Lee, I., "Plenum Chamber Effect on Wind-Tunnel Resonance by the Finite-Element Method," AIAA Journal, Vol. 26, No. 9, September 1988, pp. 1087-1093.

13. Mabey, D. G., "Resonance Frequencies of Ventilated Wind Tunnels," AIAA Journal, Vol. 18, No. 1, January 1980, pp. 7-8.

14. Ng, W. F., "Review-Simultaneous Measurements of Stagnation Temperature and Pressure Using an Aspiration Probe," Proceedings of the ASME Symposium in Pressure and Temperature Measurements, December 1986, pp. 97-104.

15. Ng, W. F., and Popernack, T. G., Jr., "Combination Probe for Hi-Frequency Unsteady Aerodynamic Measurements," IEEE Transactions on Aerospace and Electronic Systems, Vol. 24, No. 1, January 1988, pp. 76-84.

16. Mineck, R. E., personal communication, April 1988.

17. Johnson, C. B., and Stainback, P. C., "A Study of Dynamic Measurements Made in the Settling Chamber of the Langley 0.3-Meter Transonic Cryogenic Tunnel," AIAA-84-0596, Aerodynamic Testing Conference, San Diego, CA, March 1984.

18. Jones, G. S., Stainback, P. C., Harris, C. D., Brooks, C. W., and Clukey, S. J., "Flow Quality Measurements for the Langley 8-Foot Transonic Pressure Tunnel LFC Experiment," AIAA-89-0150, Aerospace Sciences Meeting, Reno, NV, January 1989.

19. Kovasznay, L. S. G., "Turbulence in Supersonic Flow," *Journal of Aeronautical Sciences*, Vol. 20, No. 10, October 1953, pp. 657-674.

20. Morkovin, M. V., "Fluctuations and Hot-Wire Anemometry in Compressible Flow," AGARDograph 24, November 1956.

21. Kline, S. J., McClintick, F. A., "Describing Uncertainties in Single-Sample Experiments," *Mechanical Engineering*, January 1953, pp. 3-7.

22. Walpole, R. E., and Myers, R. H., *Probability and Statistics for Engineers and Scientists*, 3rd ed., Macmillan, 1985, pp. 244-246.

The vita has been removed from the scanned document